Available online at www.sciencedirect.com

ScienceDirect

Deep-Sea Research II 53 (2006) 2012–2033

DEEP-SEA RESEARCH
PART II

www.elsevier.com/locate/dsr2

Patch evolution and the biogeochemical impact of entrainment during an iron fertilisation experiment in the sub-Arctic Pacific

C.S. Law[a,*], W.R. Crawford[b], M.J. Smith[a], P.W. Boyd[c], C.S. Wong[b], Y. Nojiri[d], M. Robert[b], E.R. Abraham[a], W.K. Johnson[b], V. Forsland[b], M. Arychuk[b]

[a]*National Institute for Water and Atmospheric Research (NIWA), Private Bag 14–901, Evans Bay Parade, Wellington, New Zealand*
[b]*Institute of Ocean Sciences, P.O. Box 6000, Sidney, BC, Canada V8L 4B2*
[c]*NIWA Centre for Chemical and Physical Oceanography, University of Otago, P.O. Box 56 Dunedin, New Zealand*
[d]*National Institute for Environmental Studies 16-2, Onogawa, Tsukuba, Ibaraki 305-8506, Japan*

Received 29 April 2005; accepted 4 May 2006
Available online 10 October 2006

Abstract

An in situ mesoscale iron-fertilisation experiment in the eastern sub-Arctic Pacific (SERIES) was undertaken to test the Iron Hypothesis, that increasing iron supply would stimulate phytoplankton production and particulate organic carbon (POC) export to deep water. Patch dispersion was monitored for 26 days, using an inert tracer (SF_6) and biological tracers (chlorophyll-*a* and fCO_2), and we examine the vertical and lateral evolution of the patch, and the influence of dilution on the biological and biogeochemical response to iron addition. Vertical dispersion of the added iron was initially restricted to the upper 12 m by near-surface stratification, although the vertical flux to the lower mixed layer at this time significantly exceeded the unperturbed rate of iron supply. Calculation of vertical diffusion rates (K_z) provided an estimate of the unperturbed Fe flux across the seasonal pycnocline of 0.3–1.5 nmol/m^2/d. The iron/tracer patch partially advected around an anticyclonic Haida Eddy that originated off the west coast of Canada in 1999–2000. Lateral patch evolution was initially dominated by current strain, stretching it into a filament of ~300 km^2 by day 11 and reaching a maximum area of 1300 km^2 by day 23. Sustained high winds and intrusion of external waters between days 11 and 18 altered patch geometry and advection. Two scenarios for patch evolution are presented of a single exponential dilution at 0.1/d, and a variable dilution in which dilution increased from 0.078/d to 0.16/d (days 11–18) before decreasing to 0.05/d. Dilution rates were used to constrain dissolved iron dynamics, with iron regeneration rates indirectly estimated from biological iron uptake and lateral dilution losses. Lateral entrainment supplied ~6–7 μmol/L silicic acid and 4.6 μmol/L nitrate to the patch centre by day 20, equivalent to 37% and 45%, respectively, of total biological uptake. Indirect estimates of phytoplankton nitrate uptake from patch dilution indicated a maximum rate of 1.4 μmol/L/d, in agreement with measured rates. The cumulative entrainment of 392–500 mmol dissolved inorganic carbon (DIC)/m^2 at the patch centre by day 20 was of the same order as the total biological DIC uptake and POC accumulation. The potential impacts of a mid-experiment increase in dilution were explored; these included elevated entrainment of silicic acid when concentrations in the patch were growth limiting for

---

[*]Corresponding author. Tel.: +64 43860478; fax: +64 43862153.
E-mail address: c.law@niwa.co.nz (C.S. Law).

0967-0645/$ - see front matter © 2006 Elsevier Ltd. All rights reserved.
doi:10.1016/j.dsr2.2006.05.028

phytoplankton, and decreased cell aggregation. Both factors could potentially have delayed the onset of bloom termination and export, and increased the longevity of the SERIES phytoplankton bloom.

© 2006 Elsevier Ltd. All rights reserved.

Keywords: Dilution; Iron; Phytoplankton; Nutrient limitation; Nitrate; Silicic acid

1. Introduction

Iron availability is now established as a major factor determining phytoplankton biomass and community composition in one-third of the global ocean. The first tenet of Martin's iron hypothesis, that iron availability limits growth (Martin, 1990), has been confirmed in two of the three major high-nutrient low-chlorophyll (HNLC) regions, the Equatorial Pacific and the Southern Ocean (Coale et al., 1996; Boyd et al., 2000). Several lines of evidence, including iron measurements and budgets (Martin et al., 1989), in vivo experiments (Martin et al., 1989; Boyd et al., 1996), and the coincidence of blooms with elevated aeolian Fe input (Boyd et al., 1998) indicate that the third major HNLC region, the sub-Arctic Pacific, is potentially iron-limited. This was recently confirmed by a significant increase in phytoplankton biomass in response to in situ iron addition in the Western Pacific (Tsuda et al., 2003). A subsequent in situ mesoscale iron experiment was undertaken in the Gulf of Alaska (SERIES, sub-Arctic Ecosystem Response to Iron-Enrichment Study) to confirm algal iron limitation across the sub-Arctic Pacific region. A further objective was to validate the second tenet of Martin's hypothesis, that increasing iron supply would stimulate vertical export of particulate organic carbon (POC), by monitoring the decline phase of the phytoplankton bloom. The SERIES experiment, which lasted 26 days and involved coordinated operations on three research vessels, unequivocally confirmed the first tenet, with a 15-fold increase in chlorophyll. However, whereas vertical POC export increased at the end of the experiment, only a small proportion of the total iron-induced algal carbon fixed was transferred below the permanent thermocline, with the majority being remineralised at shallow depths (Boyd et al., 2004).

The linkage between perturbation and export in SERIES demonstrates that in situ fertilisation experiments have come of age, as the framework of a mesoscale Lagrangian addition currently provides the only approach to quantitatively relate a known amount of added iron to the total carbon fixed and exported from the surface mixed-layer. The approach of in situ mesoscale addition was initially adopted for iron-limitation studies to counter the limitations of in vivo experiments in which containment and surface effects, artificial mixing and light climate and exclusion of large grazers were significant artefacts. However, unlike mesocosms or bottle experiments, in situ *iron* fertilisation experiments are unenclosed with the result that dilution of the patch negates monitoring of ecosystem response at a fixed constant iron concentration. Instead, the iron concentration and the parameters that respond to it exhibit a gradient from the fertilised patch centre (the IN station) to waters outside the patch (OUT station), with resultant exchange between the two. Recent observations from iron addition experiments have begun to highlight the importance of constraining mixing and dilution of the patch (Abraham et al., 2000; Coale et al., 2004). Mixing in the surface ocean historically has been regarded as primarily determined by diffusion (Okubo, 1971), and at certain sites, such as at the centre of an eddy where current shear is minimal, this assumption is largely correct. However, it is now recognised that horizontal dispersal of a tracer is controlled by stirring, with a tracer patch typically elongating and folding into filaments in response to local current strain (Eckart, 1948; Garrett, 1983), as observed in ocean-colour images and mesoscale tracer experiments (Abraham et al., 2000). In in situ iron fertilisation experiments the mechanism and rate of mixing will influence both the biological response to the iron and its manifestation. For example, a tracer patch that is subject to zero or low current strain will diffuse in all directions, making it easier to locate and monitor than a strain-dominated patch that evolves into a long filament. However, this may have the reverse effect in terms of biological response; dilution at an eddy centre may result in initially rapid lateral loss of added iron, or other perturbant, from the patch centre so limiting the accumulation of biomass (Law et al., 2005), whereas strain-dominated dilution may maintain primary production when macronutrients become limiting via entrainment and diffusion (Abraham et al., 2000).

Consequently the mode of patch evolution may determine the biological response, and so it is important to establish the physical mechanisms that drive patch dynamics; indeed interpretation of the impact of iron addition is critically dependent upon characterising dilution processes. In the following study, we document the temporal evolution of the SERIES iron-tracer patch using both inert and biological tracers, and derive vertical and lateral mixing rates. The factors influencing patch trajectory and dispersal are examined, and evidence presented for variation in the rate of dilution. This information is then used to examine the impact of dilution upon biogeochemical and biomass budgets, and to estimate biological iron cycling rates. In addition, we consider the impact of an increase in dilution rate on the observed biogeochemical parameters and the biological response to iron addition.

2. Methods

2.1. Site selection

Hydrodynamic and biogeochemical surveying of the region over a two-day period in early July 2002 identified the most promising site for the release at 50.14°N 144.75°W. The injection site was selected to lie close to the time-series station at Ocean Station Papa (OSP) at 50°N, 145°W, but outside the centre of neighbouring eddies, placing it in the SW sector of the eddy to the north-east of OSP (Fig. 1A,B). Site selection was based upon location of waters with low density (to minimise the possibility of subduction of the iron-enriched waters), uniform physical characteristics, low velocity and favourable direction of currents (0.25 nmiles/h, north), and typical HNLC characteristics (high macronutrients, low chlorophyll and iron-stressed phytoplankton cells as determined by photosynthetic efficiency, F_v/F_m).

2.2. Preparation and release

Approximately 5600 L of seawater were sparged with pure SF_6 en-route to the site with monitoring of SF_6 saturation at 2–3 h intervals by static equilibration of 50 ml with an equal volume of helium, and analysis by thermal conductivity detector-gas chromatography. When saturation was completed the headspace in the tanks was displaced with water to reduce degassing, and the tanks sealed. The Fe solution was prepared by addition of ~2136 kg (7680 mol) $FeSO_4 \cdot 7H_2O$ to pre-acidified (pH 1.6–1.7) ambient water from OSP in two 10,000-L tanks.

The release was coordinated and executed from the *CCGS J.P. Tully*. An ARGOS Marker Buoy drogued at 10 m was deployed at the nominal centre and monitored for a 12 h period to determine drift rate prior to release. The drifter buoy transmitted GPS position updates to the ship at 15-min intervals, providing a long-distance locator for the patch and a Lagrangian reference to correct the release track for inertial current advection during the release (Fig. 2A,B). A radar transponder on a drifter buoy was also deployed in close proximity to the ClearSat buoy as a back-up. The SF_6 and iron solutions were mixed, and then pumped aft of the vessel at 5 and 20 L/min, respectively, to a depth of ~7 m as maintained by attachment of the outlet to a fish. The release was maintained at a relatively shallow depth to avoid injection below near-surface thermal structure. The injection began at 00:50 LT on 9/07/02, with a release track describing an expanding square of 8.5×8.5 km, with 0.7 km between transect legs (Fig. 2A,B). The release was coordinated using the ship ECPINS® search and rescue package, which provided a shifting reference frame that allowed the nominal release track to be regularly re-positioned to account for advection of the central drifter buoy. Ship speed during release was ~4 knots with a total track length of 145 km over a 17.5-h period. The *JP Tully* remained outside the patch for 4 h immediately after the release to allow the SF_6 to mix vertically into the surface mixed layer.

A second release of dissolved iron without SF_6 was carried out in response to declining dissolved iron levels on 16/07/02 (day 7). An expanding rectangular track was used for the re-infusion, as the patch had elongated N–S by this stage (Fig. 2C,D). The re-infusion covered 13.1 by 6.7 km, with a total release track of 153 km, and 0.97 km between transects in a N–S direction and 0.49 km in an E–W direction. Once again the release was referenced to the position of the drifter buoy, and was coordinated using the ECPINS® system. In addition, the surface SF_6 distribution was monitored to ensure that the release was within the boundaries of the existing patch using a SF_6 threshold of 25 fmol/L, outside of which pumping of the iron tanks was

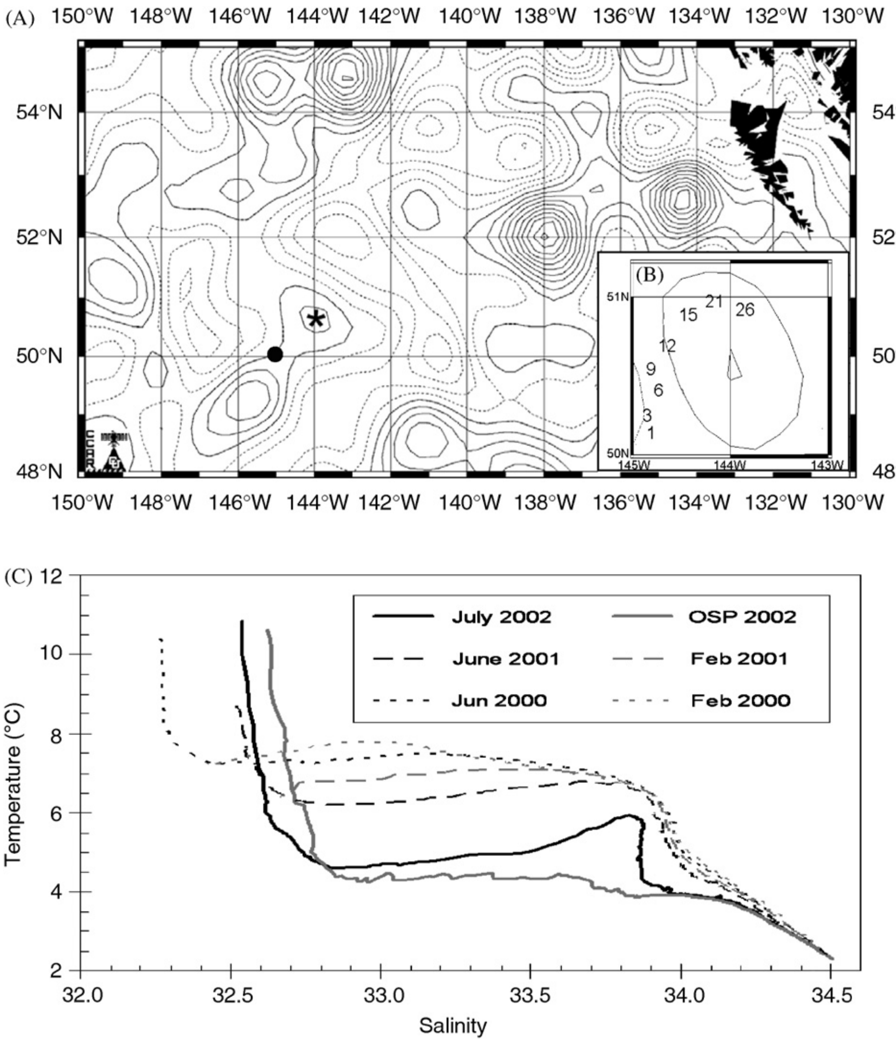

Fig. 1. (A) Contours of sea-surface height anomaly (SSHA) computed from satellite altimetry observations with a mesoscale band-pass spatial filter to remove seasonal and basin-scale features. The contour interval is 1 cm, with dashed lines denoting negative anomalies. OSP is indicated by the black circle, with the suspected remnants of the Haida-2000 eddy which the SERIES patch partially circumnavigated, labelled with *. Newer Haida and Sitka eddies are the higher-elevation features to the north. The inset (B) shows a contour plot of SSHA in early July 2002 (solid line), with patch centre positions labelled by experiment day number. All SSHA images were provided by Colorado Center for Astrodynamics Research. (C) T-S properties of the Haida-2000 Eddy between February 2000 and July 2002 (Miller et al., 2005).

suspended. The dissolved iron solution was added at a rate of 13 L/min, raising dissolved iron to ~0.6 nmol/L (Boyd et al., 2004).

2.3. Underway mapping

The patch was monitored for a period of 26 days with continual occupation throughout. Surface SF_6 and fCO_2 underway mapping were carried out aboard the *JP Tully* until day 14, and fCO_2, chlorophyll and nutrient underway mapping by the *Kaiyo-Maru* between days 16 and 26. In addition chlorophyll mapping was undertaken by *El Puma* on day 15 (Marchetti et al., 2006b). The reference Time Zero (T0) for the experiment was 0000 Local Time on 09/07/02, with events described as decimal days from this point (e.g., midday on 10/07/02 is day 1.5).

2.3.1. Surface SF_6 distribution

Surface SF_6 concentration was mapped to day 14 using surface water from the ship's intake at 5 m.

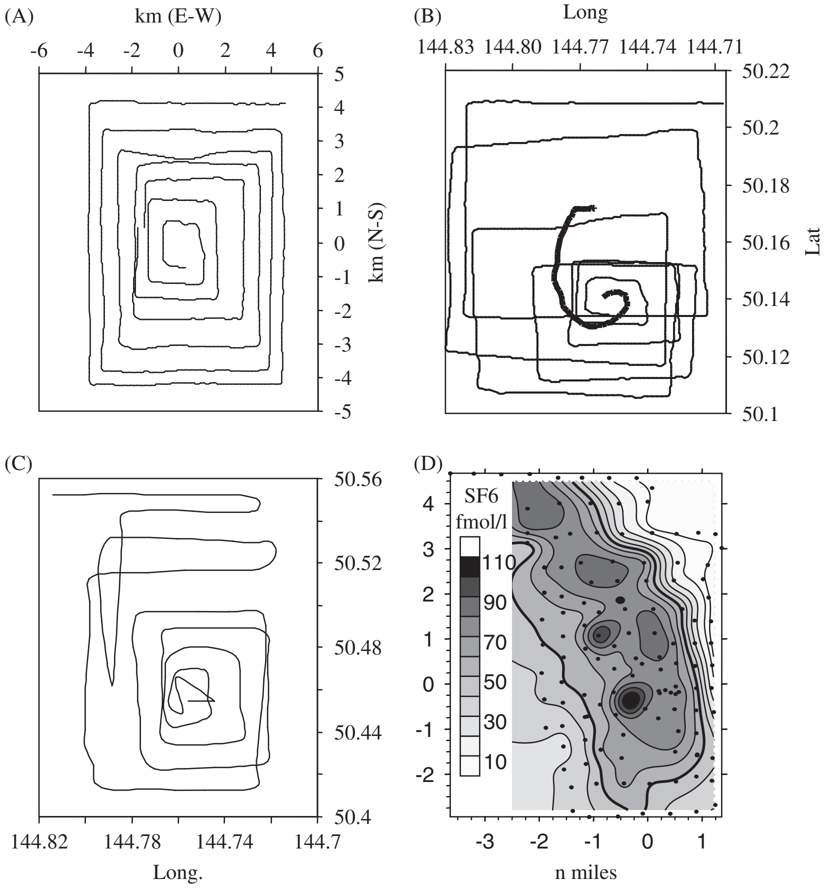

Fig. 2. (A) Nominal ship track for the initial Fe and SF_6 release, with reference drifter buoy position at 0,0. (B) Actual ship track (narrow line), and drifter buoy track (thick line) in earth coordinates during the initial Fe and SF_6 release. (C) Ship track during the second Fe release in earth coordinates. (D) Ships track during the second Fe only release, superimposed over surface SF_6 concentration in Lagrangian coordinates.

An automated mapping system extracted dissolved SF_6 by sparging with nitrogen, followed by cryogenic trapping, chromatographic separation and quantification by ECD-GC (Law et al., 1998). Each SF_6 measurement was time- and position-stamped and incorporated into a visualisation of surface SF_6 concentration relative to the ships position in Earth coordinates to enable real-time mapping. The patch was mapped on a daily basis at a ship speed of 7–10 knots for periods of 10–12 h overnight. Each SF_6 data-point was an integrated value for a period of 7 min, equivalent to a distance of ~2.2 km at a ship speed of 10 knots. Mapping was coordinated by reference to the drifter buoy position, buoy drift over the previous 12 h and the corrected Lagrangian SF_6 distribution from the previous nights mapping. The SF_6 patch elongated in an N-S direction, which required a shift in mapping strategy from a propeller track to a "Xmas-tree" track to successfully constrain the patch boundaries. Mapping of the patch became increasingly difficult from day 12 due to increased windspeeds and low SF_6. A Lagrangian correction was subsequently applied to the SF_6 data post-cruise using the relative position of the drifter buoy as a reference at each sample time, to compensate for advection of the patch by inertial and other ocean currents during mapping.

2.3.2. Surface fCO_2 distribution

Increased carbon fixation by phytoplankton in response to iron addition resulted in drawdown of carbon dioxide, so providing a biological tracer for the patch. The underway surface fCO_2 concentration was monitored at 3-min intervals, using an automated equilibrator system linked to a LICOR^{TM} infrared analyser on the *JP Tully* to day 14 (Wong et al., 2006b), and using the technique of Zeng et al. (2002) on days 17–26 aboard the *Kaiyo-Maru*. Lagrangian maps of the fCO_2 data from the *Kaiyo-Maru* were generated by reference to the GPS position of a drifter buoy that was drogued at a depth of 15 m.

2.3.3. Surface chlorophyll-a distribution

The phytoplankton response to the iron addition also elicited an increase in chlorophyll in the patch providing a further biological tracer (Marchetti et al., 2006a). This was monitored by continuous underway chlorophyll-*a* fluorescence (Chl-a) measurement at 1-minute intervals at a depth of 2 m on day 15 on the *El Puma*. Surface water fluorescence was measured using a Wet Labs WETstar flow-through fluorometer, and calibrated against discrete samples collected in the patch as described in Marchetti et al. (2006b). The underway Chl-a data were plotted in a Lagrangian framework by reference to the ARGOS position of a drifter buoy left in the patch by the *JP Tully*.

2.4. Data processing

The spatially irregular data along the ship track were mapped onto a regular grid using objective analysis. This procedure produces an optimal unbiased estimate that minimizes the mean square error in the objective estimates. Background subtraction of 5 fmol/L and 345 ppmv was applied to the SF_6 and fCO_2 data, respectively, and a sloping background concentration gradient fitted to the fCO_2 data to account for the observed gradient across the front along which the patch advected (Wong et al., 2006b). Length scales of 3.7 and 5 km were used for the SF_6 and ΔfCO_2 maps, respectively, which defined the distance that the objective mapping decreased to the noise level. The difference in length scale reflects the higher spatial resolution of fCO_2 measurements relative to SF_6 measurements. Length and width of the SF_6 patch centre were estimated for the calculation of area and strain rate by fitting Gaussian ellipsoids using unconstrained non-linear optimisation. A second estimate of the patch centre was based upon the contour line m/e, where the maximum concentration observed during each mapping period, m, declined to $1/e$. This second approach was used to examine the effectiveness of the ellipse fitting, and to obtain estimates of the patch centre area where an ellipse could not be fitted. The total patch area was estimated for SF_6, fCO_2 and Chl-a using the area enclosed by the $m/7.5$ contour in the respective objective maps.

2.5. Vertical SF_6 distribution

Vertical profiling was undertaken at IN stations at the patch centre, as identified from the SF_6 mapping data, and at OUT stations >15 km from the patch in variable directions to accommodate surrounding variability. Discrete SF_6 analysis of 300-ml water samples was achieved using a sparging technique adapted from Law et al. (1994) using manual injection. Twenty-three vertical profiles were obtained for dissolved SF_6 at IN stations between days 1 and 13, in addition to one background cast and spot samples from 10 m depth at OUT stations. The OUT station profile indicated SF_6 concentrations of 1.1–1.4 fmol/L as expected from equilibrium with the atmosphere.

3. Results

3.1. Regional hydrodynamics

Sea-surface height anomaly (SSHA) was monitored in the region of OSP for several months prior to the experiment with particular focus on the movement and position of Sitka and Haida eddies. These eddies, of ~150–300 km diameter, always rotate anti-cyclonically and are evident as positive SSHA (Crawford and Whitney, 1999; Crawford, 2002). These mesoscale features form in winter along the eastern margin of the northern Gulf of Alaska, and drift westward over periods of up to 3 years (Crawford, 2002). They are clearly visible for a period of approximately 1 year, but after this, and generally within 500 km of OSP, their amplitudes decrease to ~50 mm, which is the typical SSHA of background oceanic features. These eddies can transport coastal waters enriched in silicic acid and iron relative to that of mid-Gulf HNLC waters, out into the Gulf of Alaska (Whitney and Robert, 2002; Johnson et al., 2005; Whitney et al., 2005). By mid-summer the surface waters at the centre of these eddies are generally low in nutrients, including iron, although potential exists for re-supply during summer storms from subsurface waters (Peterson et al., 2005). As Haida and Sitka eddies occasionally reach OSP, observations were made both remotely and in-situ prior to release to avoid fertilisation of central waters within these eddies. Two persistent mesoscale features with positive SSHA near OSP were observed, one to the NE and the other to the SW of OSP (Fig. 1A). Each normally would be considered part of the background noise, but their persistence and lack of movement over several months indicated that these were anticyclonic eddies. Similar vertical temperature and salinity profiles were obtained at the core of the eddy to the SW of OSP at 49°16.97′N, 134°40.07′W and near OSP at 49°59.95′N, 144°59.90′W 5–6 days before the iron release. Evidence from tracking previous mesoscale eddy motion using altimeter-based contours of SSHA suggested the most likely identity of the eddy to the SW of OSP to be Haida-2000, which formed in the winter of 1999–2000 off the west coast of Canada. Fig. 1C shows the TS traces through this eddy at various times (Miller et al., 2005), confirming a steady evolution of eddy water toward the features of the sub-Arctic northeast Pacific Ocean.

3.2. Lateral evolution of the patch

The lateral evolution of the tracer patch was controlled at the mesoscale, primarily by a one-quarter anti-cyclonic circuit of the Haida Eddy to the NE of the initial release site. The drifter buoys and patch initially moved in a northerly direction (Figs. 1B and 3A), along a temperature and salinity front (Wong et al., 2006b). Drifter deflection during increased windspeed on day 5 was not reflected in a shift in patch track or evolution, and may have been partially attributable to wind drag on the buoy. After re-positioning at the patch centre at day 7.5, the northward buoy trajectory was maintained until day 10.5, when both drifter buoy and patch were pushed to the north–east during sustained high windspeeds. The impact of the increased winds is readily apparent when comparing the distance the buoy travelled in the 3 days prior to the high winds, of 15 km, with 35 km over the following 3 days. From day 17 the buoy was transported to the east and exhibited regular oscillations to the end of the experiment (Fig. 3A).

Overall, the patch moved anti-cyclonically, from south–west of the eddy centre on day 0 to north of the eddy centre by day 25, and so a component of the directional change was due to the rotational influence of the eddy. However, the abrupt deflection to the north–east from day 11 must reflect another influence. The oscillations exhibited by the drifter buoy reflect the inertial period at 50°N of approximately 15.7 h (Fig. 3B). The inertial and patch motion in the tracks of the drifters were separated by computing a time series of three-hourly values from fitting a function composed of a cubic polynomial plus inertial oscillation to overlapping segments of the input drifter position time series. The results indicate that the inertial speeds exceeded the patch speed over the entire period of tracking. As inertial motion transports water anti-cyclonically in the northern hemisphere, an inertial speed of 15 cm/s would transport water at 50°N around an inertial oscillation of ~1.3 km. The increase in windspeed from day 11 (Fig. 3C) prompted a surge in both inertial and non-inertial speeds, with the resulting inertial speed of 32 cm/s transporting near-surface water around a 2.8 km oscillation. This rapid increase in inertial currents may have been responsible for the change in patch direction. Inertial currents are restricted to surface layers and increasing buoyancy frequency (N^2) at the base of the mixed layer will suppress the depth penetration of inertial currents. The resulting change in inertial current speed coincident with high windspeeds may then have increased shear, and so lateral mixing and variation in mixed layer depth.

The SF_6 objective maps indicate that, from an initially square release area, the patch evolved into a filament within 48 h, and continued to elongate to a length of 32 km by day 13 (Fig. 4). The inertial oscillations were small relative to the size of the patch, and so Lagrangian correction of the mapping data did not greatly alter the distribution observed in earth coordinates, even during the periods of high windspeeds. Comparison of patch areas using advection-corrected and uncorrected data indicate differences of $<8\%$. The SF_6 maximum at the patch centre decreased from ~450 fmol/L on day 1, to 30 fmol/L by day 14 (Fig. 4). This decline was partly a function of loss to the atmosphere, which was estimated using windspeed data, mixed layer depth and the transfer velocity-windspeed parameterisations of Wanninkhof (1992) and Nightingale et al. (2000), with Schmidt number correction for temperature. A least-squares fit of the predicted trend, based on air–sea loss, to the total SF_6 for each map indicated an initial SF_6 release of ~0.5 mol (Fig. 5). Despite low winds during the first 4 days, the calculated evasion rates suggest that ~40% of the SF_6 was lost as a result of the shallow surface mixed layer at 12 m. The atmospheric loss of ~0.12/d over day 0–4 declined to 0.07/d upon mixing of the tracer to 30 m, and then to 0.026/d as windspeeds

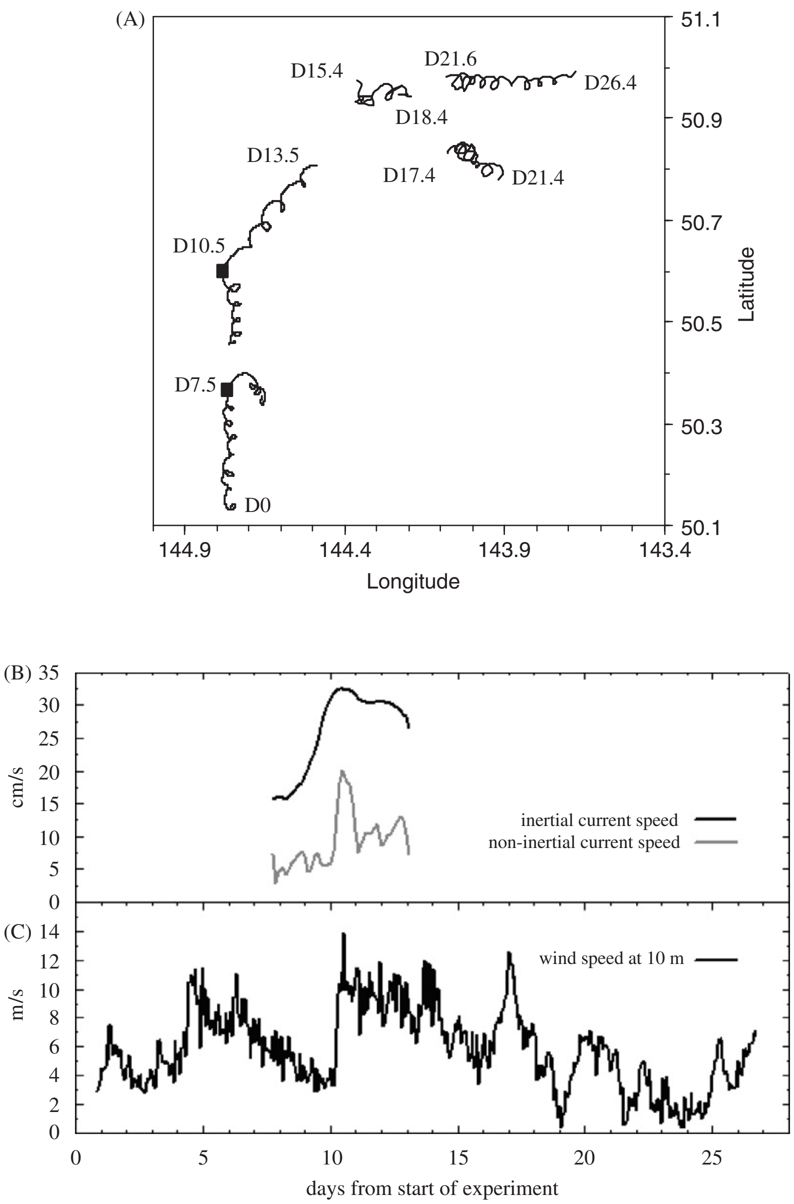

Fig. 3. (A) Drifter buoy tracks showing time of deployment and recovery. Positions between days 15 and 17 are from Argos, whereas the remainder are from direct buoy to ship transmission via uhf link. (B) Inertial speeds (black line) and non-inertial speeds (grey line) of near-surface drifters on days 7–12. (C) Wind speed data corrected to 10 m height.

decreased to 2.5 m/s, before increasing to 0.16/d during the sustained winds of days 11–14.

As lateral dispersion is largely determined by stirring associated with eddies (Garrett, 1983; Abraham et al., 2000), a tracer patch will be drawn into a filament at a rate determined by the strain rate (γ), the gradient in current velocity in the direction of the flow (Martin, 2003; McLeod et al., 2002). Initially a patch of tracer below the scale of the strain flow will spread diffusively in all directions (Garrett, 1983), but on reaching a scale of ~100 m will be stretched into a filament with the length (σ_x) increasing exponentially in response to strain. Conversely, the width (σ_y) of the patch will remain constant, maintained by the opposing thinning effect of the strain and widening due to diffusion. This stretching maintains cross-patch gradients against diffusion allowing mixing along the sides of the patch and so persistent dilution.

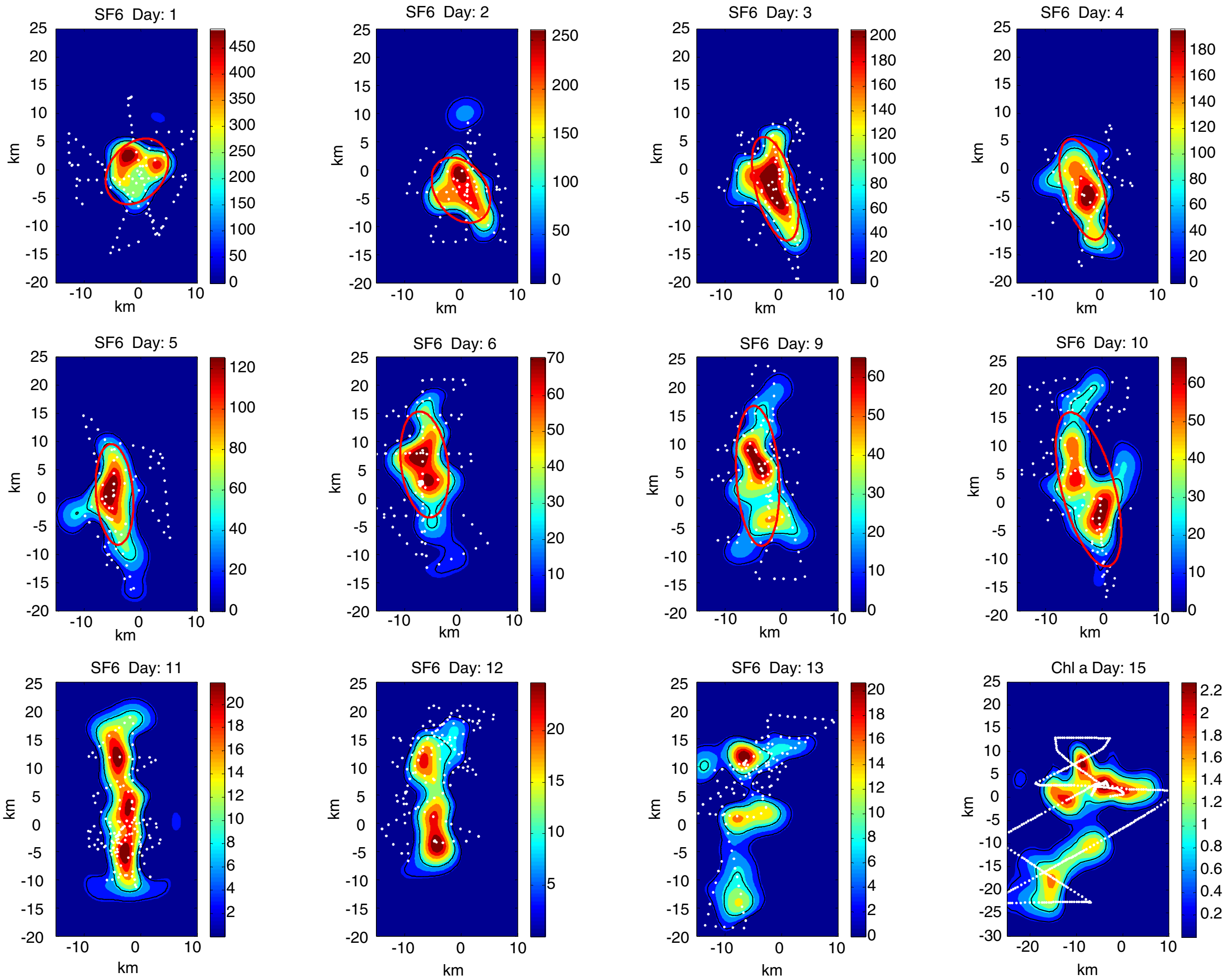

Fig. 4. Lagrangian objective maps of surface SF_6 (days 1–13, all same scale), and Chl-a (day 15.3). The x and y scales are in kilometres and the plots are referenced to the drifter buoy position at 0,0. Note that the concentration colour bar varies with each plot and the Chl-a plot on day 15 is on a different length scale. Gaussian ellipses are shown for days 1–10, but could not be fitted the SF_6 data on day 11 and the Chl-a plot on day 15. The m/e and $m/7.5$ contour lines are shown in each plot, indicating the patch centre and total patch area, respectively. Patch closure was incomplete and so areas were not subsequently used on days 12 and 13. The ships track is indicated by the white dots.

Strain and diffusion rates can be calculated from the change in the dimensions of the patch with time by fitting Gaussian ellipses to the objective maps (Abraham et al., 2000). Lengths and widths of the patch centre were determined for days 1–10 only (Fig. 7A), as elliptical Gaussians could not be fitted to the SF_6 distribution from day 11 onwards. The estimated γ value of 9.2×10^{-7}/s (~0.08/d) from the length data is consistent with the value of $8\pm3\times10^{-7}$/s (0.07/d) reported for the SOIREE iron fertilisation (Abraham et al., 2000), indicating similar dilution rates within a 14-day time frame. The filament half-width (σ_y) remained constant at ~2.9 km (Fig. 7A), from which a lateral diffusivity, K_y of 7.7 m^2/s was calculated using $K_y = {\sigma_y}^2\gamma$. This is double the diffusivity estimated for SOIREE (Abraham et al., 2000), due to the larger initial release area in SERIES, and a shallower surface mixed layer that was more susceptible to stratification and shear. Nevertheless both estimates are consistent with the range of 1–16 m^2/s determined by dye releases on similar length scales in shelf seas (Okubo, 1971).

3.3. Evidence of variation in patch evolution and dilution

Patch lengths and widths were also estimated from elliptical Gaussian fits to the ΔfCO_2 maps on

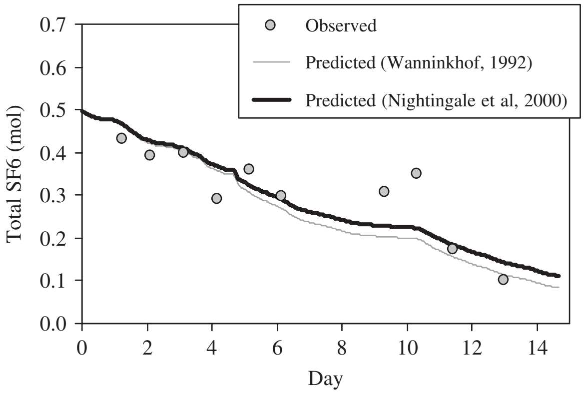

Fig. 5. Total SF_6 vs. time for days 1–14, showing observed and predicted totals based on the wind speed-gas transfer velocity parameterisations of Wanninkhof (1992) and Nightingale et al. (2000).

days 18–25 (Fig. 6). Comparison with the estimates from the SF_6 data indicated a distinct shift in patch evolution between days 11 and 18, with a doubling in filament width but no significant change in length. This is possibly because the elliptical Gaussians did not accurately fit the length of the ΔfCO_2 patch, and could not accommodate the distortion in the shape of the patch along its axis (Fig. 6). However, comparison of the patch centre areas derived from Gaussian ellipses ($2\pi\, \sigma_y\, \sigma_x$), with the estimate based upon the contour line m/e, shows generally good agreement for both SF_6 and fCO_2 (Fig. 7B). This suggests that the increase in patch centre area after day 11 was not an artefact of the Gaussian ellipse fitting, and instead that patch area increased more rapidly between day 11 and 18 than predicted from the strain-based dilution that characterised its initial evolution. This was examined further using the temporal increase in total patch area (Fig. 8). Total patch area increased from an initial area of ~100 to ~300 km^2 by day 11, with the Chl-a map on day 15.3 indicating an area of 622 km^2. The ΔfCO_2 maps on days 18–20 had a surface area of ~1000 km^2, as confirmed by an independent estimate from an ocean colour satellite image on day 20, (J. Gower, pers. comm.; Boyd et al., 2004), with total patch area reaching a maximum of ~1300 km^2 by day 23. Total patch area declined after day 24; which may reflect the difficulty of mapping a large area or alternatively declining drawdown of fCO_2 as indicated by a second ocean colour image on day 24 (Boyd et al., 2004). Although the minimum fCO_2 at the patch centre on days 25–26 was not significantly different from that observed on days 18–24 (Wong et al.,2006b), and windspeeds were too low to induce significant air–sea exchange, it is likely that a combination of diminishing biological drawdown (Boyd et al., 2004), and mixing with external waters of elevated fCO_2 negated further expansion of the fCO_2 patch after day 24.

Both patch centre and total area estimates indicate an increase in the rate of dilution after day 11 (Figs. 7 and 8). It is evident that the increase in dilution coincided with the shift from conservative SF_6 tracer to biological tracers; however, areal estimates of both parameters on day 12 did not differ (SF_6 224 km^2; fCO_2, 212 km^2). Although this is not an ideal comparison, as the biological signal was strengthening as the SF_6 declined towards background concentrations, this indicates that the change in dilution was real and did not arise from a switch in mapping parameter. If the patch had continued to dilute at a rate of 0.078/d, as observed for the first 11 days, the predicted total patch area would be ~645 km^2 on day 20, whereas the actual total patch area was 80% greater (~1026 km^2 in ΔfCO_2 maps and ~1000 km^2 in the ocean colour image). Between days 18–24 the calculated area from the fCO_2 maps exceeded the predicted area by ~60% (Fig. 8). Fitting a single exponential (subsequently referred to as 1-*ED*) to the total patch areas for SF_6 (to day 10), Chl-a (day 15) and ΔfCO_2 (to day 25) provided a dilution rate of ~0.1/d, with a 95% c.i. of 0.093–0.106 (Fig. 8). The uncertainty was estimated using a bootstrapping approach by sampling the distribution with replacement 5000 times. Although the 1-*ED* provided a reasonably robust fit it is based on the assumption that areal evolution of the patch, and so dilution, remained constant throughout the 26 days of the experiment. An alternative interpretation using a variable exponential fit (subsequently referred to as 3-*ED*) was obtained by fitting single exponentials to the periods between day 0 and 11.43 ($a1$), and day 18.1 to 25 ($a3$). The dilution rates were 0.078 (0.059–0.010)/d for $a1$, and 0.05 (0.035–0.07)/d for $a3$, with the 95% confidence intervals estimated by bootstrapping. Assuming that rapid dilution occurred between $a1$ and $a3$, we can estimate the dilution required in $a2$ by interpolating between the two curves. From the bootstrap data the patch area was 330 (303–381) km^2 at day 11.43 and 964 (902–1030) km^2 on day 18.1, giving a dilution rate for $a2$ of 0.16 (0.13–0.18)/d (Fig. 8). The 1-*ED*

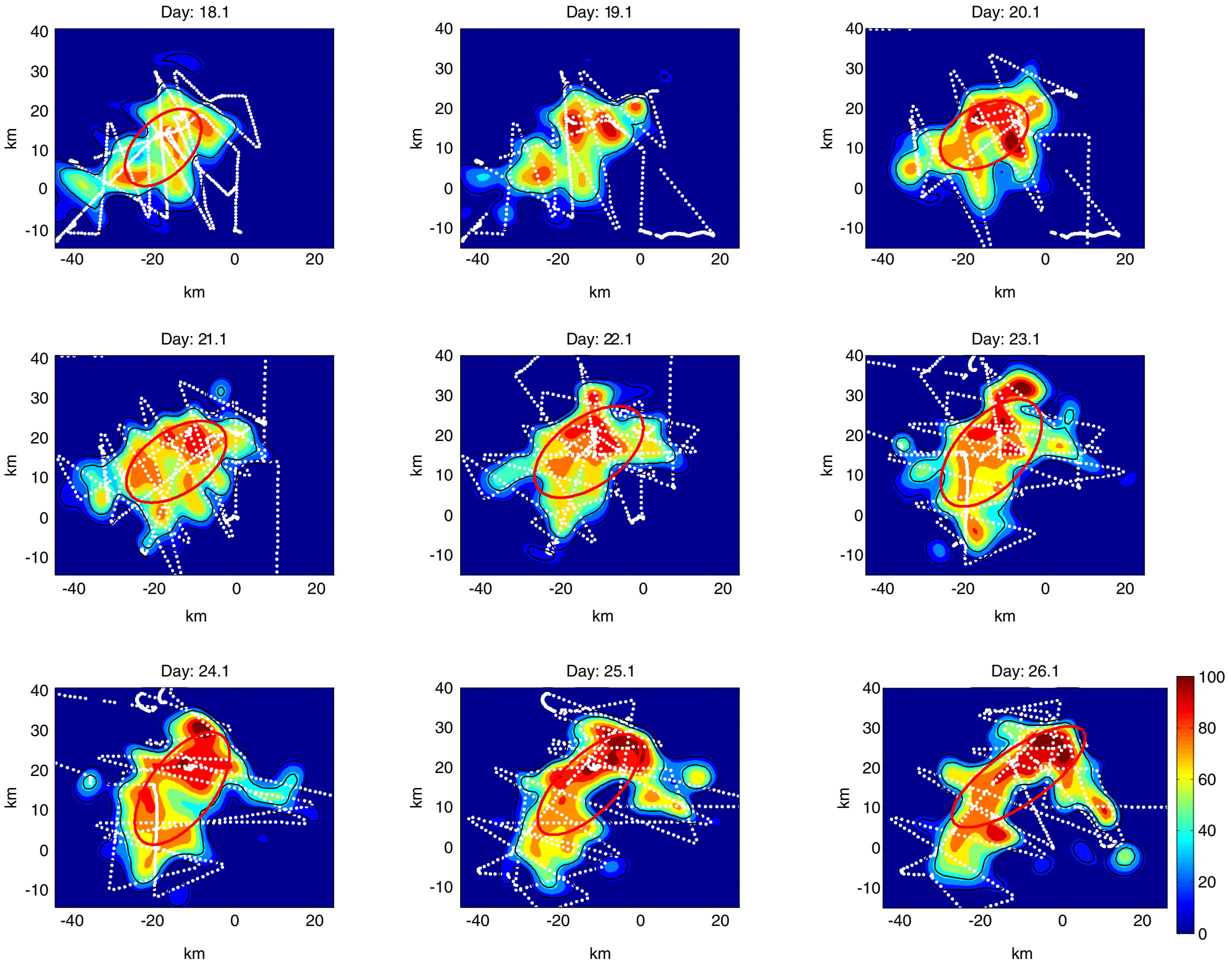

Fig. 6. Lagrangian objective maps of surface ΔfCO_2 for days 18–26. All ΔfCO_2 maps have the same x and y length scale and concentration scale, and are referenced to the drifter buoy position at 0,0. The ΔfCO_2 was calculated by subtraction of a background (345 ppm) and a sloping background concentration gradient was also fitted for the observed gradient in fCO_2 across the patch. Gaussian ellipse fits are shown for all days except day 19. The m/e and $m/7.5$ contour lines are shown in each plot, indicating the patch centre and total patch area, respectively. The ships track is indicated by the white dots.

dilution rate is consistent with that recorded for the SOIREE and SoFex patches (Abraham et al., 2000; Coale et al., 2004), whereas the higher dilution rate in the 3-*ED* is consistent with a dilution rate of 0.2/d for a SF_6 tracer patch in sub-Antarctic waters (Croot et al., submitted for publication). Despite the apparent consistency observed in previous experiments, the variation in dilution rate in SERIES is perhaps not too surprising. This is not only because SERIES provided the longest observational dataset of patch evolution to date, but also because strain in ocean currents is highly variable both spatially and temporally, and so there is no reason to expect stretching of a filament to remain constant indefinitely (Sundermeyer and Price, 1998). Whereas either dilution scenario provides a reasonable fit to the dataset, the 3-*ED* indicates a doubling in dilution after day 11 relative to 1-*ED*, which would influence the timing and magnitude of the biological and biogeochemical responses to the iron addition.

Evidence of a change in patch evolution and dilution after day 11 was also apparent in the patch geometry. The increase in total patch area may reflect folding of the filament, as indicated by the doubling in the width of the patch centre between days 11 and 17 (Fig. 7A). Variation in patch geometry was apparent from analysis of the aspect ratio of both patch centre and total patch areas. If current strain remained constant and uniform the aspect ratio of an initially circular patch, estimated

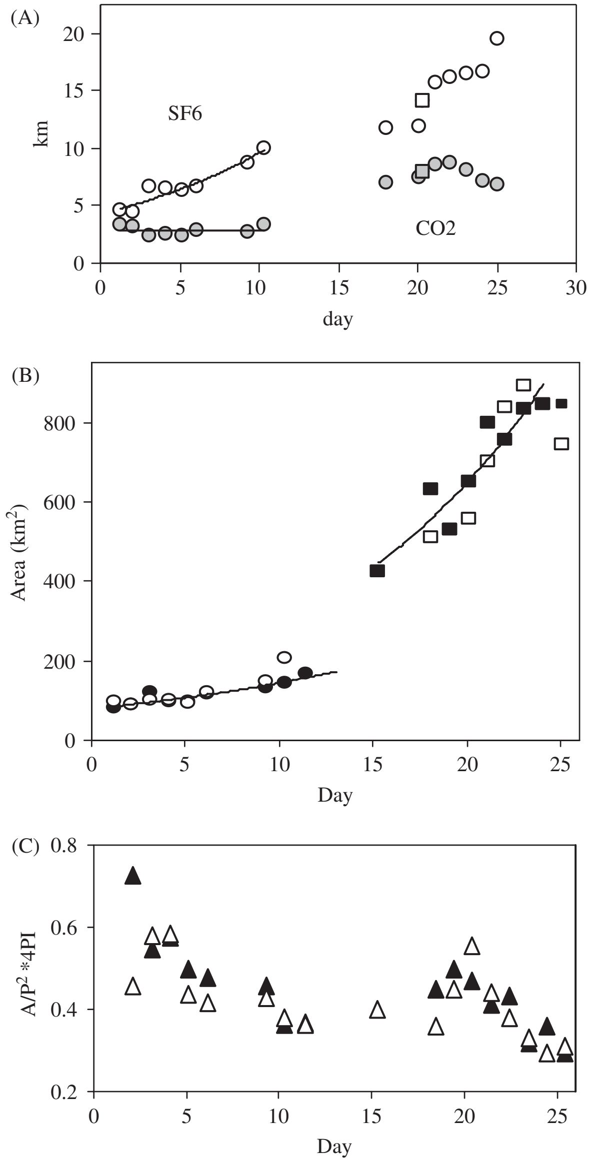

Fig. 7. (A) Length (σ_x) (open symbols) and widths (σ_y) (grey symbols) of Gaussian ellipses fitted to the objectively mapped SF_6 data (days 1–10), and ΔfCO_2 data (days 18–26) for the patch centre. The squares indicate the length and width of the Chl-a patch in the ocean colour image on day 20.4. (B) Surface areas of the patch centre estimated from Gaussian ellipses (white symbols) for days 1–10 for SF_6 maps and days 18, 20–26 for ΔfCO_2 maps, and m/e contours (black symbols) fitted to objectively-mapped SF_6 data (days 1–11), Chl-a (day 15) and ΔfCO_2 data (day 18–26). (C) Aspect ratio of the patch centre (black diamonds) and total patch (white diamonds) estimated from the m/e contour data as area/(perimeter)^2, and normalised to 1 for an idealised circular patch by multiplying by 4π.

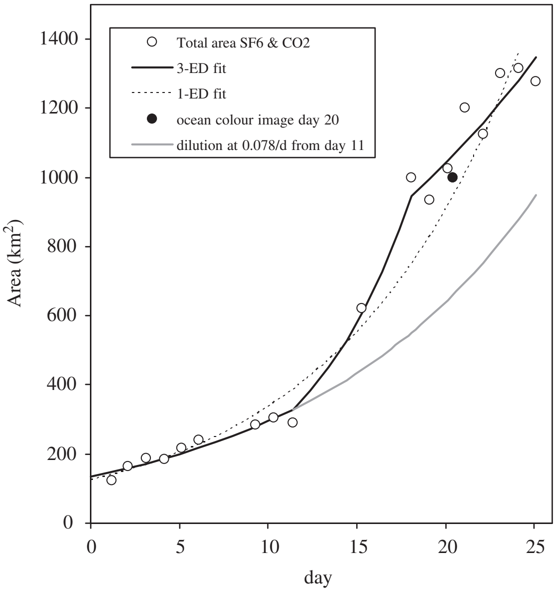

Fig. 8. Total patch area (white circles) at a dilution rate of 0.1/d (*1-ED*, dashed line), and for *3-ED* (solid line) from fitting exponentials to data between days 0–11.43, days 11.43–18.1, and days 18.1–25 separately. The predicted surface area had dilution continued at 0.078/d after day 11 is included (grey line), and the surface area derived from an ocean colour image on day 20 (black circle) is also shown. Closure of patch boundaries for SF_6 on days 12–14, and fCO_2 on day 17 was incomplete, and so total areas were not considered for these days. Day 26 is also omitted from the exponential fits.

as the Area/Perimeter^2 and scaled using a factor of 4π, would decrease uniformally from 1 as the patch stretched into a filament. This was the case until day 10 after which the aspect ratio of both patch centre and total patch areas increased to day 19–20, indicating that the patch became more spherical and less filamentous during this period (Fig. 7C).

Further evidence of folding and intrusion events was apparent in surface contour plots. Deformation of the patch occurred during the period of sustained high windspeeds from day 10, with intrusion of cooler water from the west and warmer water from the east in the SF_6 surface distribution on day 13, coincident with deflection of the northern part of the patch to the NE (Fig. 9). It should be noted that coverage of the SF_6 patch was limited at this stage, and objective maps for days 12–14 were not used to estimate patch area. Information on the lateral distribution of the patch was limited between days 14–17, with the only map on day 15 of Chl-a indicating that the southern part of the patch had pivoted and folded at the constriction point observed on day 13 (Fig. 4). However, this interpretation is based on relatively limited spatial coverage of the patch. There is also indirect evidence of intrusion into the patch from the biogeochemical data. Increases in dissolved nitrate and phosphate (2–2.5 and 0.2 μmol/L, respectively) were observed at certain IN station casts during day 12–14, in contrast to the general decline in macronutrients during this period (Marchetti et al., 2006b). As IN station selection was based on maximum Chl-a at this stage, the IN stations were unlikely to have been incorrectly identified, particularly as background Chl-a levels were uniformly low, and so this is interpreted as indicative of intrusion of high nutrient water. A corresponding increase in mixed-layer δ^{15}N-nitrate at this time was possibly due to both vertical and lateral entrainment (Needoba et al., 2006). The decrease in surface fCO_2, which had been apparent from day 8, plateaued between day 10 and 14, consistent with fCO_2 drawdown by algal fixation being offset by entrainment of high fCO_2 waters from outside the patch. However, fCO_2 was also influenced by increased air-sea exchange and CO_2 production during calcification during this period (Wong et al., 2006b).

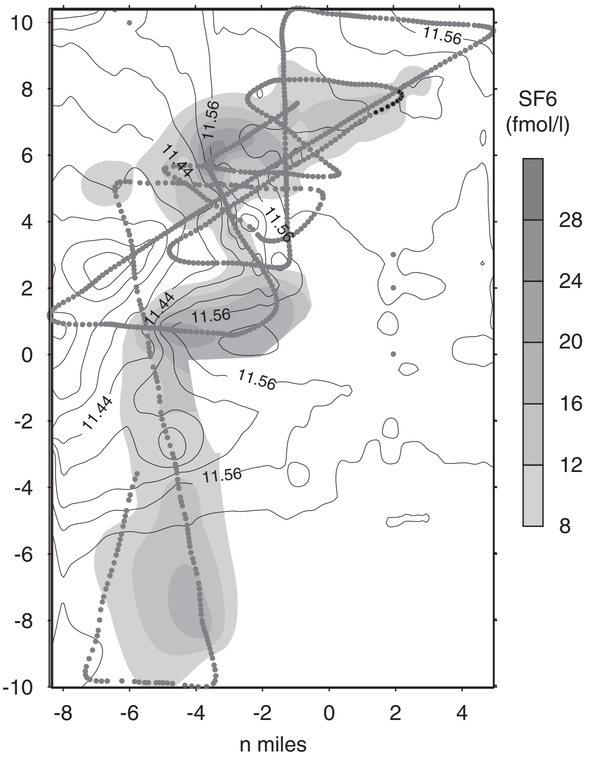

Fig. 9. Surface SF_6 concentration (colour bar) overlaid on temperature (contour lines) with ship track indicated (grey dots) on day 13.

Intrusion of external water into the patch was also apparent on day 18, with a tongue of cool water extending S–SE across the patch lowering surface temperature and raising both fCO_2 (Fig. 10) and dissolved nutrients (data not shown) at the patch centre. By day 20 this intrusion had been completely encircled by the patch, but was still evident as a temperature minimum with elevated fCO_2, nitrate and silicic acid at the patch centre. This folding is analogous to the mechanism described by Garrett (1983), in which an inert tracer filament, having increased in length beyond that of the local eddy scale, folds over on itself entrapping tracer-free water. However, this is generally considered to occur over longer timescales when variability in the strain field has divided the original filament into a number of sub-filaments. Overall, the evidence suggests that, whereas current strain dictated the evolution of the patch during the initial stages of the experiment, wind-driven advection and shear caused vertical and lateral intrusion leading to folding and enhanced dilution during days 11–17. Unfortunately, ADCP current velocity data were not available for confirmation of the dynamic processes that determined patch evolution.

The lack of continual monitoring of an inert conservative tracer for the full 26 days of the experiment is a hindrance to the interpretation. Use of biological tracers of the fertilised patch that are non-conservative is not ideal, particularly as the biological tracers Chl-a and fCO_2 may respond on different temporal scales. However, comparison of the Chl-a and ΔfCO_2 maps during days 18–26 shows no significant difference in patch shape or surface area. Theoretically, an exponentially-increasing biological tracer will describe a Gaussian with the same variance as an inert tracer, as demonstrated by Martin (2003), and supported by observational data on the evolution of the SOIREE patch (Abraham et al., 2000). The distribution of a biological and inert tracer may diverge when growth rate and strain rate differ significantly (McLeod et al., 2002), but only in a system that is not nutrient-limited. A non-linear biological response to dissolved iron concentration could, however, introduce an artefact to the estimate of total patch area when based upon Chl-a or fCO_2. Observations from previous iron fertilisation experiments have identified a dissolved iron threshold of ~0.2 fmol/L above which phytoplankton growth is not limited, as confirmed for SERIES (Boyd et al., 2005). In SOIREE this resulted in a “top-hat effect” of relatively constant

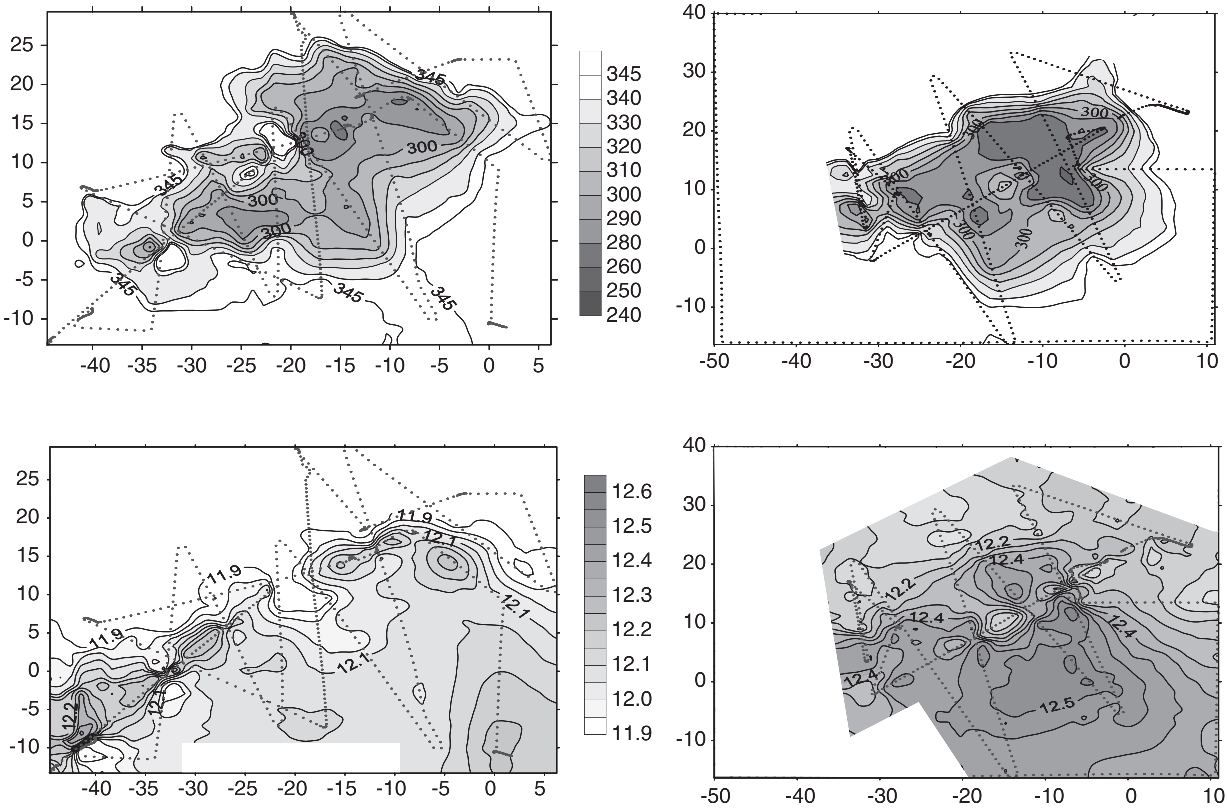

Fig. 10. Contour plots of fCO_2 (top) and temperature (bottom) on days 18 (left) and 20 (right), with the ship track indicated by dots. The upper colour bar for fCO_2 (ppm) applies to both upper plots, and the lower temperature (°C) colour bar applies to both lower plots. Note the change in length scale in both *x*- and *y*-axis between day 18 and 20 plots.

fCO_2 and F_v/F_m across the patch (Bakker et al., 2001; Boyd and Abraham, 2001). This non-linearity could artificially increase the area of a biological tracer, such as fCO_2 or Chl-a, relative to an inert tracer such as SF_6 that exhibits a Gaussian distribution. However, a top-hat effect was not readily apparent in the SERIES fCO_2 data (Fig. 6; Wong et al., 2006b), suggesting that algal carbon uptake was linearly related to dissolved iron and so SF_6 concentration¸ as observed in IronExII (Cooper et al., 1996; Bakker et al., 2001).

3.4. *Vertical evolution of the tracer patch*

SF_6 concentration decreased throughout the experiment due to dilution and volatilisation, although near-surface concentrations remained initially high due to restricted vertical mixing imposed by near-surface stratification. This stratification was evident as a maximum in the buoyancy frequency, N^2, which intensified during days 2–3 and coincided with a Tracer Layer Depth (TLD; the depth at which SF_6 decreased to 50% of the average in overlying water) of 10–12 m (Fig. 11B). Although weaker than at the base of the seasonal mixed layer this structure was sufficient to prevent the vertical transfer of SF_6 and iron into the lower surface-mixed layer. The near-surface stratification persisted due to relatively low initial windspeeds (mean 4.7 m/s), but was eroded as windspeed increased to 13 m/s on day 5 (Fig. 11A). This resulted in a "classical" mixed layer of uniform N^2 and SF_6 concentration down to the seasonal pycnocline at 28 m (Fig 11B,C). Windspeeds declined over the following 4–5 days during which structure reformed at 10–15 m, and then increased to ~13–14 m/s on day 10.5, remaining relatively constant until the departure of the *JP Tully* on day 14. This increase in windspeed coincided with decoupling of SF_6 and density at the base of the seasonal mixed layer, on days 11 and 12 (Fig. 11B) indicative of lateral intrusion.

The vertical diffusion coefficient (K_z), was calculated from the increase in the second moment (M2),

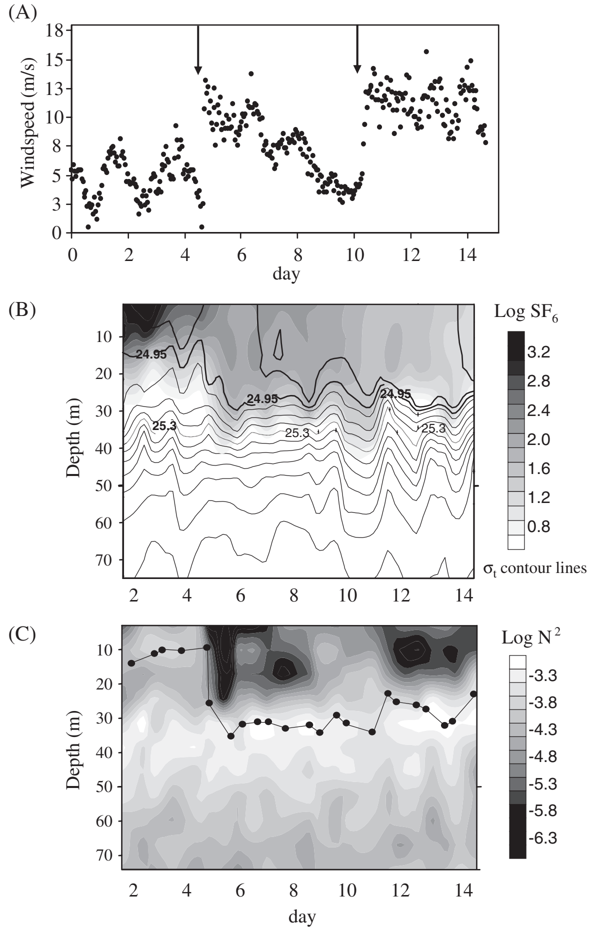

Fig. 11. (A) Mean hourly windspeed in m/s to day 14, with the two wind events indicated by vertical arrows. (B) Depth contour plot of log SF_6 concentration overlain on density (σ_t) contours to day 14. (C) Depth contour plot of log N^2 with the TLD indicated by the dotted line to day 14.

by fitting half-Gaussians to the SF_6 distribution at the base of the TLD (Law et al., 1998, 2003). Separate K_z estimates were obtained for days 1–4, when SF_6 was maintained at depths <14 m, and days 5–9 when SF_6 had mixed down to ~28 m. Penetration of SF_6 across the weak stratification at 12 m was apparent in the four depth profiles to day 4, from which a K_z of $1.12 \pm 0.47 \times 10^{-4}\,m^2/s$ was calculated. Between days 5 and 9 the SF_6 distribution closely matched the isopycnals, with limited penetration into the seasonal pycnocline. Consequently, the K_z determined from the increase in M2 with time in seven SF_6 profiles during this period (Fig. 12), of $0.14\ (\pm 0.10) \times 10^{-4}\,m^2/s$, was an order of magnitude lower than on days 1–4. This reflected the elevated N^2 at the base of the mixed layer, and possibly also the near-surface stratification on days 7–9 (Fig. 11C) that restricted transfer of energy from the surface to the base of the mixed layer. It also should be noted that vertical shear in the horizontal currents may have obscured or ameliorated accumulation of SF_6 in the pycnocline (Law et al., 2003), and that the spatial resolution was relatively coarse, at 5 m depth intervals. However, both K_z estimates show reasonable agreement with the K_z–N^2 trend reported for other tracer experiments (Law et al., 2003).

3.5. Vertical iron and macronutrient exchange

Although near-surface stratification restricted the transfer of the added iron into the lower surface-mixed layer during days 1–4, the high Fe gradient at 10–12 m would have maintained supply via vertical diffusion to the lower surface-mixed layer. The calculated K_z and observed Fe gradient between 7.5 and 20 m of 188 nmol/m^4 (Wong et al., 2006a) could sustain a flux of 1–2.6 μmol Fe/m^2/d that would have supplied 0.07–0.14 nmol Fe/l/d to the lower mixed layer (14–30 m) during this period. Thus, despite retention of the majority of the added Fe in the upper 12 m, the vertical diffusive flux into the lower mixed layer exceeded the combined supply from vertical diffusion across the seasonal pycnocline (9.5 nmol Fe/m^2/d), and dust deposition (0.16 μmol Fe/m^2/d) reported at OSP (Martin et al., 1989). Although no change was observed in Chl-a below 12 m on days 1–4 (Marchetti et al., 2006a), there was evidence of a small but significant increase in F_v/F_m during this period (R. Strzepek, pers. comm.), indicating that the vertical iron flux at this time was sufficient to stimulate physiological

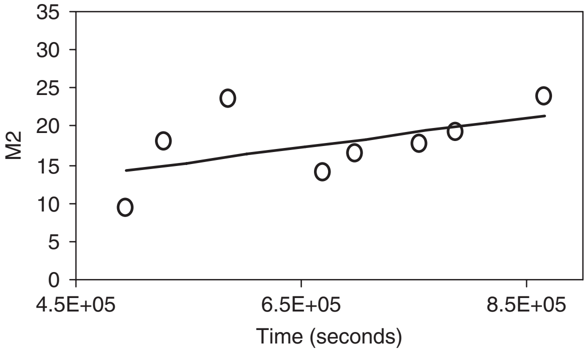

Fig. 12. A linear fit to the increase in the second moment, M2, of SF_6 profiles at the base of the mixed layer between day 5 and 9 for calculation of K_z (Law et al., 1998, 2003).

changes in the phytoplankton in the lower mixed layer. Following wind-induced mixing to 30 m on day 5 dilution and scavenging lowered mixed layer dissolved iron concentrations (Wong et al., 2006a). The resulting dissolved Fe gradient at the base of the seasonal mixed layer during days 5–9 of ~21 nmol Fe/m^4 would have sustained a diffusive loss of 7–43 nmol Fe/m^2/d, corresponding to a decrease of 0.2–1.4 pmol Fe/l/d in the mixed layer.

Under non-perturbed conditions sub-pycnocline water represents a source of dissolved Fe to the surface mixed layer in the sub-Arctic Pacific. Assuming that the vertical diffusion rate recorded for days 5–9 is representative of the region, the cross-pycnocline supply of iron could be calculated using dissolved Fe profiles at the OUT stations (Wong et al., 2006a). The dissolved Fe gradient at 20–40 m of 0.75 nmol/m^4 could support a vertical flux of 0.3–1.5 nmol Fe/m^2/d (0.01–0.05 pmol Fe/L/d), 6–30 times lower than previous estimates (Martin et al., 1989). The nitrate and silicic acid concentration gradients of 176 and 348 μmol/m^4 across the seasonal pycnocline would sustain a vertical supply of 0.06–0.36 and 0.12–0.72 mmol/m^2/d, respectively, equating to increases of 2–12 and 4–24 nmol/L/d in an unperturbed system. The Si:NO$_3$ flux ratio was 2, intermediate between the iron-deplete and iron-replete Si:NO$_3$ ratios observed during SERIES (Boyd et al., 2005). The Si:NO$_3$ flux ratio was also significantly lower than that calculated for the ACC (Law et al., 2003), which may reflect differences in source water stoichiometry, phytoplankton composition and nutrient uptake or differential regeneration rates.

4. Discussion

4.1. Patch dilution and dissolved iron dynamics

A previous study of the fate of added iron during an in situ mesoscale experiment identified dilution as the major pathway for the decline in dissolved Fe (Bowie et al., 2001). The initial addition of iron during SERIES raised dissolved Fe concentrations to ~2 nmol/L at day 1.6, but this had decreased to ~0.7 nmol/L by day 3.8 (Boyd et al., 2004; Wong et al., 2006a). Dilution at 0.078–0.1/d would account for ~25–31% of this decrease, with non-conservative loss processes such as oxidation, scavenging onto particles and biological uptake responsible for the remainder (Bowie et al., 2001; Wong et al., 2006a). Vertical mixing of the patch to 28 m on day 5 resulted in further dilution of dissolved Fe, necessitating a second release on day 8 that increased concentrations to ~0.6 nmol/L (Boyd et al., 2004). Dissolved Fe concentrations fell sharply over the following 24 h (Wong et al., 2006a), but then declined conservatively with dilution between days 9.5 and 12 (Fig. 13A).

The biota were physiologically iron-replete until day 11–12 when dissolved Fe fell below the critical threshold of 0.2 nmol/L, after which there was a 4–5 day transition period to algal Fe limitation as indicated by F_v/F_m. Yet, net primary production rates continued to increase to day 14 and algal stocks increased for a further 5–6 days (Boyd et al., 2005). This continued increase in phytoplankton production required either an increase in biological Fe uptake and/or utilisation of intra-cellular iron (Takeda et al., 2006). Dissolved Fe decreased by 55% between day 12 and 14, at a rate that exceeded the high dilution in 3-*ED* (Fig. 13A). This non-conservative loss may have resulted from an increase in particle scavenging and loss associated with intrusion of water from outside the patch, or alternatively an increase in biological uptake. To account for the latter, phytoplankton Fe uptake rates were calculated using the observed primary production rates (Marchetti et al., 2006c), and a Fe:C molar ratio of 5×10^{-6} characteristic of iron-deplete HNLC regions (Twining et al., 2004). This indicated a maximum Fe uptake of ~33 pmol/L/d on day 13 (see Fig. 13B), 2–3 times greater than Fe uptake rates during the SOIREE iron fertilisation experiment (Bowie et al., 2001). The predicted dissolved Fe concentration, based on dilution losses and phytoplankton uptake, showed good agreement with the observed data between days 12 and 14, supporting the case for an increase in Fe uptake after day 11. However, lower dissolved Fe concentrations were predicted from day 14 onwards than observed, due either to a decrease in Fe:C uptake ratio (Twining et al., 2004), and/or the exclusion of a Fe regeneration term in this simple model. Assuming the latter, the discrepancy between observed and predicted Fe concentration from day 12 in Fig. 13A was used to estimate maximum Fe regeneration rate, which peaked at 25 pmol/L/d on day 14 (Fig. 13B). This is higher than reported in SOIREE (Bowie et al., 2001), but comparable to rates in unperturbed HNLC waters (Strzepek et al., 2005). The similarity in the magnitude of Fe uptake and regeneration suggests tight coupling, consistent with observations from other iron fertilisation

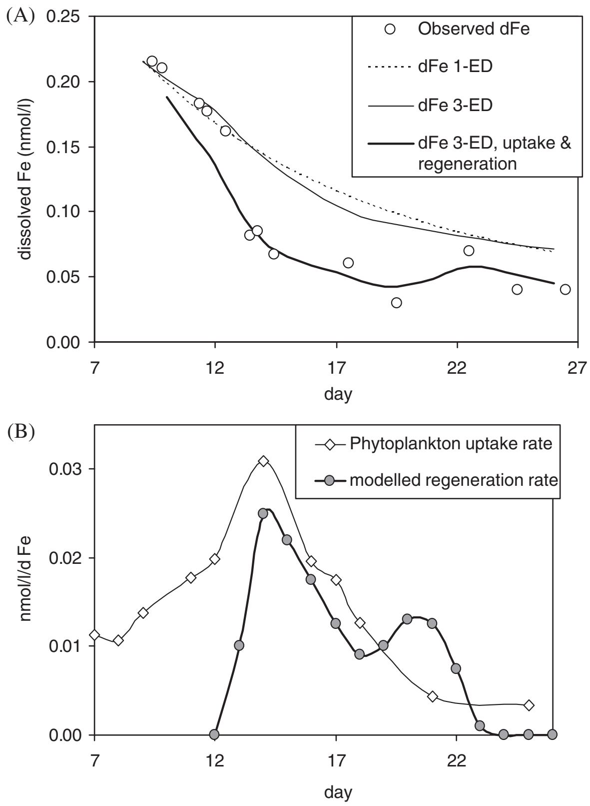

Fig. 13. (A) Observed dissolved iron concentration, dFe (Wong et al., 2006a) for days 7–26, with predicted concentration based on dilution in the 1-*ED* (dashed line) and 3-*ED* (narrow line) scenarios, and with 3-*ED* plus biological uptake and modelled regeneration (thick line). (B) Biological Fe uptake rates (white diamonds) estimated from a Fe:C of 5×10^{-6}, (Twining et al., 2004) and SERIES primary production rates (Marchetti et al., 2006c), and the maximum Fe regeneration rate (grey circles), estimated from the discrepancy between predicted and observed dFe.

experiments and non-perturbated Lagrangian studies of Fe dynamics (Bowie et al., 2001; Strzepek et al., 2005).

4.2. Patch dilution and macronutrient availability

The trends in dissolved nutrients inside and outside the SERIES patch are described in detail elsewhere (Timothy et al., 2006; Saito et al., 2006). Variability in dissolved nitrate and silicic acid at OUT stations arose from the location of the patch on a front between water masses of differing biogeochemical composition (Wong et al., 2006b), resulting in variability in the IN/OUT macronutrient gradient in the initial phase of the experiment. In addition, concentrations of macronutrients declined at OUT stations over the course of the 26-day experiment (Boyd et al., 2004; Saito et al., 2006). Significant nutrient drawdown in the patch was apparent from day 8, with silicic acid and nitrate falling to <10% and 50% of their initial values by day 20. Macronutrient entrainment was calculated by applying the dilution rate to the IN/OUT nutrient gradient, using the 5 m nutrient data (Boyd et al., 2004) to minimise the influence of stratification, shear, and vertical gradients in nutrients and phytoplankton uptake (Marchetti et al., 2006b). Entrainment increased sharply after day 11 (Fig. 14A,B) and peaked when IN patch silicic acid and nitrate concentrations were lowest on day 18–19. Maximum entrainment rates were 0.75–1.5 μmol/L/d for silicic acid and 0.6–0.7 μmol/L/d for nitrate, with cumulative entrainment totals of ~6–7 μmol/L silicic acid and 4.4–4.8 μmol/L nitrate by day 20. Phytoplankton nutrient uptake was indirectly calculated using the predicted conservative nutrient concentration following correction for dilution, and subtracting the observed nutrient concentration on each day (Fig. 14A,B). Uptake rates showed some variability, with maximum silicate uptake at ~3.5 μmol/L/d on days 12 and 15. Although direct measurements of uptake rate were not made, silicic acid uptake rates of 1.75 and 0.75 μmol/L/d were estimated for day 12 and 17 from Si:NO_3 ratios and algal growth rates (Boyd et al., 2005; Takeda et al., 2006). Maximum nitrate uptake of 1.3–1.4 μmol/L/d was in good agreement with measured rates (^{15}N-nitrate uptake in bottle incubations that were not subject to dilution), which peaked at 1.5 μmol/L/d on day 15 (Marchetti et al., 2006b).The estimated cumulative biological uptake was 17–18 μmol/L silicic acid and 10.1–10.4 μmol/L nitrate by day 20 (Fig. 14C), of which entrainment supplied 37% and 45%, respectively. The latter showed good agreement with cumulative nitrate uptake estimated from measured rates, of 12.05 μmol/L (Marchetti et al., 2006b; Needoba et al., 2006). The ratio of cumulative silicic acid uptake to cumulative nitrate uptake increased to ~2 around day 14 in response to the transition from iron-replete to deplete conditions (Boyd et al., 2005; Takeda et al., 2006).

The biological response to the Fe addition resulted in an increase in POC and decrease in dissolved inorganic carbon (DIC) due to algal carbon fixation, and also an increase in dissolved organic carbon (DOC) as a result of exudation and grazing. From day 8, when carbon fixation in the patch began to exceed that outside, dilution resulted

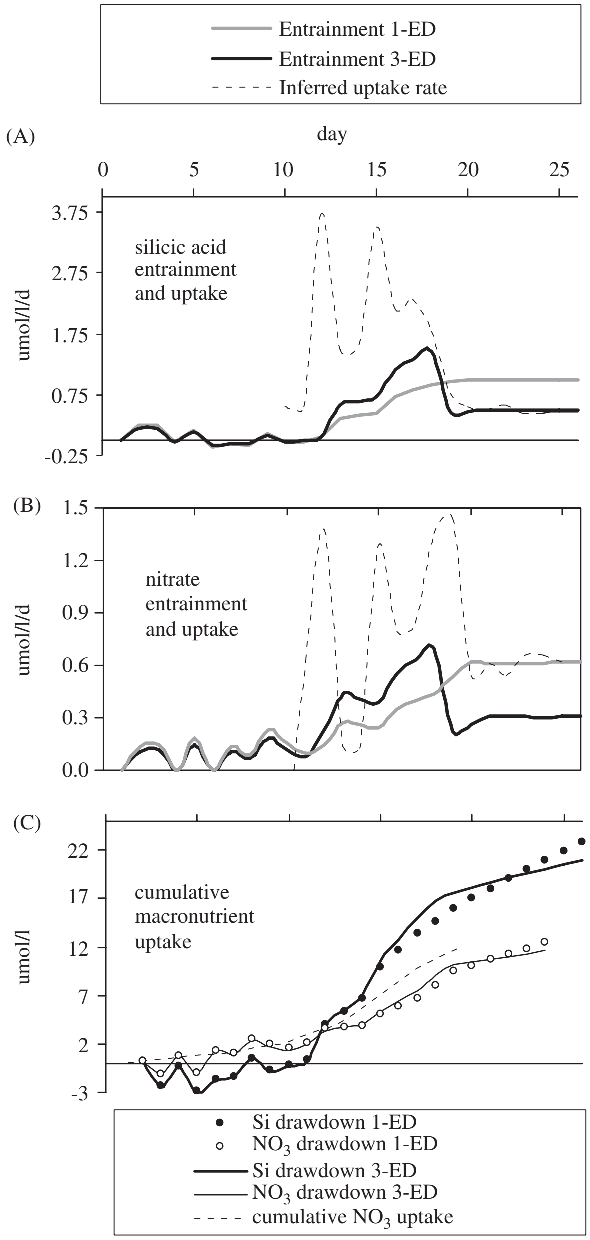

Fig. 14. (A) Silicic acid entrainment at the patch centre, estimated from dilution by 1-*ED* (grey line) and 3-*ED* (thick line), with inferred silicic acid uptake rate using 3-*ED* (dashed line). (B) Nitrate entrainment estimated from dilution by 1-*ED* (grey line) and 3-*ED* (thick line), with inferred nitrate uptake rate estimated using 3-*ED* (dashed line). IN station nutrient data on day 13 were excluded from the entrainment calculation. (C) Cumulative silicic acid (1-*ED* black circles; 3-*ED* thick line) and nitrate (1-*ED* white circles; 3-*ED* narrow line) drawdown, with cumulative nitrate uptake (dashed line) from ^{15}N-nitrate uptake measurements (Marchetti et al., 2006b; Needoba et al., 2006).

in lateral loss of POC, and DOC in the later stages of the experiment, and entrainment of DIC. Variability in the waters surrounding the patch and general warming of surface waters resulted in temporal and spatial variability in the IN/OUT DIC gradient (Wong et al., 2006b). After accounting for this variability, dilution of the patch resulted in a cumulative POC loss of ~9.4 mmol/m^3, DOC loss of ~2.6 mmol/m^3 and DIC gain of ~21.7 mmol/m^3, and so a net supply of 9.7 mmol/m^3 C to the patch centre by day 20 (Fig. 15A). These results translate to a cumulative gain of 392–500 mmol DIC/m^2 and lateral loss of 157–193 mmol POC/m^2 and 25–50 mmol DOC/m^2, when accounting for shoaling of the patch towards the end of the experiment (Saito et al., 2006; Timothy et al., 2006). Combining the observed DIC deficit at the patch centre and the cumulative DIC entrained provides an estimate of maximum biological DIC drawdown at the patch centre of ~64 mmol/m^3 on day 18 (Fig. 15B). The net result of dilution was an increase of 210–257 mmol DIC/m^2; combining this with the observed DIC deficit of 163 mmol DIC/m^2 at the patch centre indicates a total biological uptake of 373–450 mmol DIC/m^2 by day 20, consistent with the reported POC accumulation of 328 mmol POC/m^2 on day 18 (Boyd et al., 2004). These calculations confirm that the lateral exchange of carbon species was significant, in the case of DIC exceeding vertical carbon export and other loss terms (Table 1, Boyd et al., 2004) by an order of magnitude. This emphasises the importance of considering dilution and entrainment in carbon and macronutrient budgets in mesoscale Lagrangian experiments.

4.3. The impact of change in dilution rate on the biological response of the bloom

A change in patch dynamics, as in *3-ED*, would alter biogeochemical pools within the patch and influence the observed response to iron addition. Dissolved Fe concentrations in the patch were relatively low by day 12, being only double that outside the patch, and so a change in dilution between days 11 and 18 may not have significantly altered iron dynamics. However, it is notable that the temporal trend in the predicted dissolved Fe with 3-*ED* shows greater correspondence with the observed values (Fig. 13A). Similarly, a change in dilution rate influenced DIC to the extent that 20% more DIC was entrained with 3-*ED* than 1-*ED* by day 18 (Fig. 15B). However, this would not have impacted phytoplankton growth and production, as DIC was not limiting.

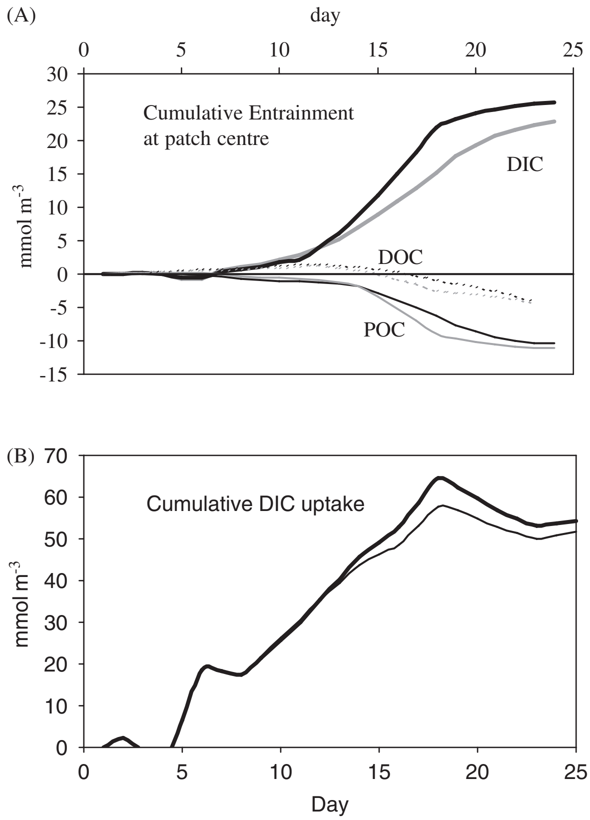

Fig. 15. (A) Impact of dilution upon dissolved and particulate carbon species at the patch centre, showing entrainment of DIC (thick line) and loss of DOC (dashed line) and POC (narrow line), using 1-*ED* (grey) and 3-*ED* (black). (B) Cumulative biological DIC uptake estimated using 1-*ED* (narrow line) and 3-*ED* (thick line) dilution scenarios.

Although the total amount of silicic acid and nitrate entrained showed little difference between the two dilution scenarios, 3-*ED* would support 30–50% greater nutrient entrainment during the period of maximum phytoplankton growth between day 12 and 18 (Fig. 14A,B). Entrainment during this period would supply the equivalent of 82% of the biological silicic acid uptake in 3-*ED,* but only 40% in the 1-*ED* scenario. Fig. 14A shows that silicic acid entrainment in the 3-*ED* scenario would exceed the modelled uptake rate of 0.75 μmol/L/d between days 15 and 18, whereas entrainment only equal uptake by day 18 in the 1-*ED*. This would significantly influence bloom longevity as silicic acid had decreased to <10% of the initial IN station concentration by day 18, and was physiologically limiting (Marchetti et al., 2006b; Saito et al., 2006), with concentrations below the 1 μmol/L threshold required for diatom growth (Martin-Jézéquel et al., 2000). Consequently the 3-*ED* scenario could maintain silicic acid supply during the period when phytoplankton growth was still active (Boyd et al., 2005), whereas silicic acid supply would only become significant with 1-*ED* as the bloom approached termination. Abraham et al. (2000) previously demonstrated that entrainment could maintain phytoplankton production in an iron-fertilised patch when silicic acid is drawn down to growth-limiting concentrations, in a manner analogous to a chemostat (Boyd and Law, 2001). Coale et al. (2004) have also identified the importance of entrainment in maintaining phytoplankton growth in an iron-fertilised patch in low silicic acid HNLC waters to the north of the Polar Front. For SERIES we speculate that increased dilution between day 11 and 18 could have sustained phytoplankton production during peak carbon fixation and growth via entrainment of silicic acid, extending the longevity and magnitude of the biological response. Conversely, had dilution remained under strain-dominated control at a rate of 0.078/d the bloom may have terminated at an earlier stage due to silicic acid limitation. Furthermore, the inferred decrease in dilution and silicic acid entrainment after day 18 in the 3-*ED* scenario could have precipitated bloom decline and vertical POC export, as was observed (Boyd et al., 2004), further supporting the case for physical evolution of the patch as a major driver of bloom development and termination.

4.4. The impact of change in dilution rate on bloom termination

Accumulation of phytoplankton biomass occurs when the net growth rate exceeds dilution. During days 1–12, when the mean algal growth rate was 0.2/d (Boyd et al., 2005), dilution at 0.078/d resulted in a loss of ~27% of stocks associated with algal growth. Growth rate subsequently increased to 0.4/d, when dilution at the 3-*ED* rate would have resulted in ~37% loss; consequently the increased dilution in the 3-*ED* scenario would not have prevented biomass accumulation at the patch centre. Conversely an increase in dilution may have sustained accumulation, by reducing the potential for algal aggregation which is the precursor for bloom decline and POC export (Jackson and Lochmann, 1992). This can be demonstrated by estimating the diatom cell biovolume had dilution remained at 0.078/d instead of increasing to 0.16/d in the 3-*ED* scenario, which would have resulted in a 25% greater cell biovolume by day 18 (Fig. 16). Cell contact and aggregation will increase in a bloom to a critical cell biovolume threshold where bloom termination is initiated (Jackson and Lochmann, 1992), which was estimated to be 2.3 ppm in SERIES (Boyd et al., 2005). Had dilution remained at 0.078/d the cell biovolume would have significantly exceeded this threshold at an earlier stage (Fig. 16), resulting in earlier aggregation and vertical export. It may be further speculated that an increase in dilution under 3-*ED* would delay bloom termination via other mechanisms including lowering Transparent Exopolymer Particle abundance so reducing cell stickiness. This is consistent with a modelling study of bloom termination, in which minimisation of dilution in an iron-induced diatom bloom resulted in the onset of aggregation at an earlier stage (Boyd et al., 2002). Although these results do not confirm either dilution scenario, they demonstrate that an increase in dilution would delay both macronutrient limitation and cell aggregation, and suggest that the apparent increase in dilution during SERIES could have maintained the bloom by delaying termination and subsequent vertical POC export.

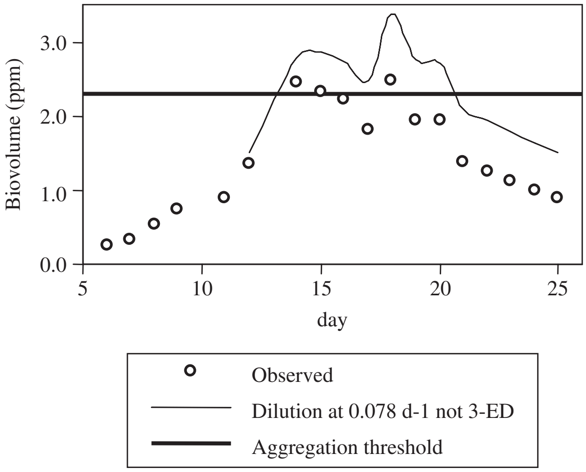

Fig. 16. Observed diatom biovolume (Boyd et al., 2005), with predicted biovolume (narrow line), had dilution remained at 0.078/d from day 11 instead of increasing at 3-*ED*. Predicted biovolumes were calculated by multiplying the observed value by the difference in dilution rate, and adding the respective observed increase in biovolume between each day. The solid horizontal line is the modeled critical threshold of 2.3 ppm above which cell aggregation would be initiated (Boyd et al., 2005).

Acknowledgements

SERIES was an ambitious experiment that was successfully achieved due to the considerable efforts of a number of people, and we gratefully acknowledge the efforts of all SERIES personnel. In particular, aboard the *JP Tully*, we thank Tim Soutar for preparation and coordination of the Fe and SF_6 release, Rousilon Chichkin for assistance with the underway SF_6 mapping, Janet Barwell-Clarke and Frank Whitney for nutrient data, Nes Sutherland for dissolved iron measurements and Doug Anderson for CTD operations. We also thank Nelson Sherry and Adrian Marchetti on the *El Puma* for nutrient and chlorophyll data, and Hiroaki Saito, Atsushi Tsuda and J. Nishioka for biogeochemical and hydrodynamic data from the *Kaiyo-Maru.* We also acknowledge the assistance and professionalism of the Captains, officers and crews of the three research vessels the C*CGS J.P. Tully*, *the El Puma*, and the *Kaiyo-Maru.* In addition we thank Doug Yelland and John Page for data manipulation.

References

Abraham, E.R., Law, C.S., Boyd, P.W., Lavender, S.J., Maldonado, M.T., Bowie, A.R., 2000. Importance of stirring in the development of an iron-fertilized phytoplankton bloom. Nature 407, 727–730.

Bakker, D.C.E., Watson, A.J., Law, C.S., 2001. Southern Ocean iron enrichment promotes inorganic carbon drawdown. Deep-Sea Research II 48, 2483–2507.

Bowie, A.R., Maldonado, M.T., Frew, R.D., Croot, P.L., Achterberg, E.P., Mantoura, R.F.C., Worsfold, P.J., Law, C.S., Boyd, P.W., 2001. The fate of added iron during a mesoscale fertilisation experiment in the Southern Ocean. Deep-Sea Research II 48, 2703–2743.

Boyd, P.W., Abraham, E.R., 2001. Iron-mediated changes in phytoplankton photosynthetic competence during SOIREE. Deep-Sea Research II 48 (11–12), 2529–2550.

Boyd, P.W., Law, C.S., 2001. The Southern Ocean Iron Enrichment experiment (SOIREE)—introduction and overview. Deep-Sea Research II 48 (11), 2425–2438.

Boyd, P.W., Muggli, D.L., Varela, D.E., Goldblatt, R.H., Chretien, R., Orians, K.J., Harrison, P.J., 1996. In vitro iron enrichment experiments in the NE Subarctic Pacific. Marine Ecology Progress Series 136 (1–3), 179–193.

Boyd, P.W., Wong, C.S., Merrill, J., Whitney, F., Snow, J., Harrison, P.J., Gower, J., 1998. Atmospheric iron supply and enhanced vertical carbon flux in the NE subarctic Pacific: is there a connection? Global Biogeochemical Cycles 12 (3), 429–441.

Boyd, P.W., Watson, A.J., Law, C.S., Abraham, E.R., Trull, T., Murdoch, R., Bakker, D.C.E., Bowie, A.R., Buesseler, K.O., Chang, H., Charette, M., Croot, P., Downing, K., Frew, R., Gall, M., Hadfeild, J., Harvey, M., Jameson, G., La Roche, J., Liddicoat, M., Ling, R., Maldonado, M.T., McKay, M., Nodder, S., Pickmere, S., Pridmore, R., Rintoul, S., Safi, K., Sutton, P., Strzepek, R., Tannenberger, K., Turner, S., Waite, A., Zeldis, J., 2000. A mesoscale phytoplankton bloom in the polar Southern Ocean stimulated by iron fertilization. Nature 407, 695–702.

Boyd, P.W., Jackson, G.A., Waite, A.M., 2002. Are mesoscale perturbation experiments in polar waters prone to physical artefacts? Evidence from algal aggregation modelling studies. Geophysical Research Letters 29 (11), 1541, doi:10.1029/2001GL014210.

Boyd, P.W., Law, C.S., Wong, C.S., Nojiri, Y., Tsuda, A., Levasseur, M., Takeda, S., Rivkin, R., Harrison, P.J., Strzepek, R., Gower, J., McKay, R.M., Abraham, E., Arychuk, M., Barwell-Clarke, J., Crawford, W., Crawford, D., Hale, M., Johnson, K., Kiyosawa, J., Kudo, I., Marchetti, A., Miller, W., Needoba, J., Nishioka, J., Ogawa, J., Page, J.T., Robert, M., Saito, H., Sastri, A., Sherry, N., Soutar, T., Sutherland, N., Taira, Y., Whitney, F., Wong, S.K.E., 2004. The decline and fate of an iron-induced subarctic phytoplankton bloom. Nature 428, 549–553.

Boyd, P.W., Strzpek, R., Takeda, S., Jackson, G., Wong, C.S., McKay, R.M., Law, C.S., Kiyosawa, H., Saito, H., Sherry, N., Johnson, K., Gower, J., Ramaiah, N., 2005. The evolution and termination of an iron-induced mesoscale bloom in the North East subarctic Pacific. Limnology and Oceanography 50 (6), 1872–1886.

Coale, K.H., Johnson, K.S., Fitzwater, S.E., Gordon, R.M., Tanner, S., Chavez, F.P., Ferioli, L., Sakamoto, C., Rogers, P., Steinberg, M.F.P., Nightingale, P., Cooper, D., Cochlan, W.P., Landry, M.R., Constantinou, J., Rollwagen, G., Trasvina, A., Kudela, R., 1996. A massive phytoplankton bloom induced by an ecosystem-scale iron fertilization experiment in the equatorial Pacific Ocean. Nature 383, 495–501.

Coale, K.H., Johnson, K.S., Chavez, F.P., Buesseler, K.O., Barber, R.T., Brzezinski, M.A., Cochlan, W.P., Millero, F.J., Falkowski, P.G., Bauer, J.E., Wanninkhof, R.H., Kudela, R.M., Altabet, M.A., Hales, B.E., Takahashi, T., Landry, M.R., Bidigare, R.R., Wang, X.J., Chase, Z., Strutton, P.G., Friederich, G.E., Gorbunov, M.Y., Lance, V.P., Hilting, A.K., Hiscock, M.R., Demarest, M., Hiscock, W.T., Sullivan, K.F., Tanner, S.J., Gordon, R.M., Hunter, C.N., Elrod, V.A., Fitzwater, S.E., Jones, J.L., Tozzi, S., Koblizek, M., Roberts, A.E., Herndon, J., Brewster, J., Ladizinsky, N., Smith, G., Cooper, D., Timothy, D., Brown, S.L., Selph, K.E., Sheridan, C.C., Twining, B.S., Johnson, Z.I., 2004. Southern ocean iron enrichment experiment: Carbon cycling in high- and low-Si waters. Science 304, 408–414.

Cooper, D.J., Watson, A.J., Nightingale, P.D., 1996. Large decrease in ocean-surface CO_2 fugacity in response to in situ iron fertilization. Nature 383, 511–513.

Crawford, W.R., 2002. Physical characteristics of Haida Eddies. Journal of Oceanography 58 (5), 703–713.

Crawford, W.R., Whitney, F., 1999. Mesoscale eddies aswirl with data in Gulf of Alaska Ocean, EOS. Transactions of the American Geophysical Union 80 (33), 365–370.

Croot, P.L., Frew, R. D., Sander, S., Hunter, K.A., Ellwood, M., Abraham, E.R., Law, C.S., Smith, M.J., Boyd, P. W., submitted for publication. The effects of physical forcing on iron chemistry and speciation during the FeCycle experiment in the South West Pacific. Global Biogeochemical Cycles, submitted for publication.

Eckart, C., 1948. An analysis of stirring and mixing in incompressible fluids. Journal Marine Resources 7, 265–275.

Garrett, C., 1983. On the initial streakiness of a dispersing tracer in two- and three-dimensional turbulence. Dynamics of Atmospheres and Oceans 7, 265–277.

Jackson, G.A., Lochmann, S.E., 1992. Effect of coagulation on nutrient and light limitation of an algal bloom. Limnology Oceanography 37, 77–89.

Johnson, W.K., Miller, L.A., Sutherland, N.E., Wong, C.S., 2005. Iron transport by mesoscale Haida eddies in the Gulf of Alaska. Deep-Sea Research II 52 (7–8), 933–953.

Law, C.S., Watson, A.J., Liddicoat, M.I., 1994. Automated vacuum analysis of sulphur hexafluoride in seawater: Derivation of the atmospheric trend (1970–1993) and potential as a transient tracer. Marine Chemistry 48 (1), 57–69.

Law, C.S., Watson, A.J., Liddicoat, M.I., Stanton, T., 1998. Sulphur hexafluoride as a tracer of biogeochemical and physical processes in an open-ocean iron fertilisation experiment. Deep-Sea Research II 45, 977–994.

Law, C.S., Abraham, E.R., Watson, A.J., Liddicoat, M.I., 2003. Vertical eddy diffusion and nutrient supply to the surface mixed layer of the Antarctic Circumpolar Current. Journal Geophysical Research—Oceans 108 (C8) art. no. 3272, C8.

Law, C.S., Abraham, E.R., Woodward, E.M.S., Liddicoat, M.I., Fileman, T.W., Thingstad, T.F., Kitidis, V., Zohary, T., 2005. The fate of phosphate in a Lagrangian enrichment experiment in the Eastern Mediterranean. Deep-Sea Research II 52 (22–23), 2911–2927.

Marchetti, A., Sherry, N.D., Kiyowsa, H., Tsuda, A., Harrison, P. J., 2006a. Phytoplankton Processes during a Mesoscale Iron Enrichment in the NE Subarctic Pacific: Part I–Biomass and Assemblage. Deep-Sea Research II, this issue [doi:10.1016/j.dsr2.2006.05.038].

Marchetti, A., Juneau, P., Whitney, F.A., Wong, C.S., Harrison, P. J., 2006b. Phytoplankton Processes during a Mesoscale Iron Enrichment in the NE Subarctic Pacific: Part II–Nutrient Utilization. Deep-Sea Research II, this issue [doi:10.1016/j.dsr2.2006.05.031].

Marchetti, A., Sherry, N.D., Juneau, P., Strzepek, R.F., Harrison, P. J., 2006c. Phytoplankton Processes during a Mesoscale Iron Enrichment in the NE Subarctic Pacific: Part III: Primary Productivity. Deep-Sea Research II, this issue [doi:10.1016/j.dsr2.2006.05.032].

Martin, J.H., 1990. Glacial-interglacial CO_2 change: the iron hypothesis. Paleoceanography 5 (1), 1–13.

Martin, A.P., 2003. Phytoplankton patchiness: the role of lateral stirring and mixing. Progress in Oceanography 57, 125–174.

Martin, J.H., Gordon, R.M., Fitzwater, S.B.W.W., 1989. VERTEX: phytoplankton/iron studies in the Gulf of Alaska. Deep-Sea Research I 36 (5), 649–680.

Martin-Jézéquel, V., Hildebrand, M., Brzezinski, M., 2000. Silicon metabolism in diatoms: implications for growth. Journal of Phycology 36, 821–840.

McLeod, P., Martin, A.P., Richards, K.J., 2002. Minimum length for growth-limited oceanic plankton distributions. Ecological Modelling 158, 111–120.

Miller, L.A., Robert, M., Crawford, W.R., 2005. The large, westward-propagating Haida Eddies of the Pacific eastern boundary. Deep-Sea Research II 52 (7–8), 845–851.

Needoba, J.A., Marchetti, A., Henry, M. F., Harrison, P.J., Wong, C.S., Johnson, W.K., Pederson, T.F., 2006. Stable nitrogen isotope dynamics of a mesoscale iron enrichment experiment in the NE Subarctic Pacific. Deep-Sea Research II, this issue [doi:10.1016/j.dsr2.2006.05.021].

Nightingale, P.D., Malin, G., Law, C.S., Watson, A.J., Liss, P.S., Liddicoat, M.I., Boutin, J., Upstill-Goddard, R.C., 2000. In situ evaluation of air-sea gas exchange parameterizations using novel conservative and volatile tracers. Global Biogeochemical Cycles 14 (1), 373–387.

Okubo, A., 1971. Oceanic diffusion diagrams. Deep-Sea Research I 18, 789–802.

Peterson, T.D., Whitney, F.A., Harrison, P.J., 2005. Macronutrient dynamics in an anticyclonic mesoscale eddy in the Gulf of Alaska. Deep-Sea Research II 52 (7–8), 909–932.

Saito, H., Tsuda, A., Nojiri, Y., Nishioka, J., Takeda, S., Kiyosawa, H., Kudo, I., Noiri, Y., Tsuneo, O., Taira, Y., Suzuki, K., Yoshimura, T., Boyd, P. W., 2006. Nutrients and phytoplankton dynamics during the stationary and declining phases of a phytoplankton bloom induced by iron-enrichment in the eastern subarctic Pacific. Deep-Sea Research II, this issue [doi:10.1016/j.dsr2.2006.05.029].

Strzepek, R.F., Maldonado, M.T., Higgins, J., Hall, J., Wilhelm, S.W., Safi, K., Boyd, P.W., 2005. Spinning the ferrous wheel—the importance of the microbial community in an Fe budget. Global Biogeochemical Cycles, 19(4), GB4S26, doi:10.1029/2005GB002490.

Sundermeyer, M.A., Price, J.F., 1998. Lateral mixing and the North Atlantic Tracer Release Experiment: observations and simulations of Lagrangian particles and a passive tracer. Journal Geophysical Research 103, 21481–21497.

Takeda, S., Yoshi, N., Boyd, P.W., Yamanaka, Y., 2006. Modeling studies investigating the causes of preferential depletion of silicic acid relative to nitrate during SERIES, a mesoscale iron enrichment in the NE subarctic Pacific. Deep-Sea Research II, this issue [doi:10.1016/j.dsr2.2006.05.027].

Timothy, D.A., Wong, C. S., Nojiri, Y., Ianson, D.A., Whitney, F.A., 2006. The effects of patch expansion on budgets of C, N and Si for the Subarctic Ecological Response to Iron Enrichment Study (SERIES). Deep-Sea Research II, this issue [doi:10.1016/j.dsr2.2006.05.042].

Tsuda, A., Takeda, S., Saito, H., Nishioka, J., Nojiri, Y., Kudo, I., Kiyosawa, H., Shiomoto, A., Imai, K., Ono, T., Shimamoto, A., Tsumune, D., Yoshimura, T., Aono, T., Hinuma, A., Kinugasa, M., Suzuki, K., Sohrin, Y., Noiri, Y., Tani, H., Deguchi, Y., Ogawa, T.N.H., Fukami, K., Kuma, K., Sano, T., 2003. A mesoscale iron enrichment in the western Subarctic Pacific induces a large centric diatom bloom. Science 300, 958–961.

Twining, B.S., Baines, S.B., Fisher, N.S., 2004. Element stoichiometries of individual plankton cells collected during the Southern Ocean Iron Experiment (SoFeX). Limnology Oceanography 37, 2115–2128.

Wanninkhof, R., 1992. Relationship between wind speed and gas exchange over the ocean. Journal Geophysical Research 97 (C5), 7373–7382.

Whitney, F.A., Robert, M., 2002. Structure of Haida eddies and their transport of nutrient from coastal margins into the Pacific Ocean. Deep-Sea Research I 46, 2351–2370.

Whitney, F.A., Crawford, D.W., Yoshimura, T., 2005. The uptake and export of silicon and nitrogen in HNLC waters of the NE Pacific. Deep-Sea Research II 52 (7–8), 1055–1067.

Wong, C.S., Johnson, W.K., Sutherland, N., Nishioka, J., Robert, M., Takeda, S., 2006a. Iron speciation and dynamics during SERIES, a Mesoscale Iron Enrichment Experiment in the NE Pacific. Deep-Sea Research II, this issue [doi:10.1016/j.dsr2.2006.05.037].

Wong, C.S., Timothy, D.A., Law, C.S., Nojiri, Y., Xie, L., Wong, S.-K.E., Page, J.S., 2006b. Carbon distribution and fluxes during the SERIES iron fertilization experiment with special reference to the fugacity of carbon dioxide (fCO_2). Deep-Sea Research II, this issue [doi:10.1016/j.dsr2.2006.05.036].

Zeng, J., Nojiri, Y., Murphy, P.P., Wong, C.S., Fujinuma, Y., 2002. A comparison of pCO_2 distributions in the northern North Pacific using results from a commercial vessel in 1995–1999. Deep-Sea Research II 49, 5303–5315.